Current developments in MRI for assessing rodent models of multiple sclerosis

ARTICLE *in* FUTURE NEUROLOGY · JULY 2014

DOI: 10.2217/fnl.14.33

5 AUTHORS, INCLUDING:

Maree T Smith

University of Queensland

239 PUBLICATIONS **3,121** CITATIONS

SEE PROFILE

Ian M. Brereton

University of Queensland

131 PUBLICATIONS **1,343** CITATIONS

SEE PROFILE

Graham John Galloway

University of Queensland

120 PUBLICATIONS **1,932** CITATIONS

SEE PROFILE

Nyoman D. Kurniawan

University of Queensland

74 PUBLICATIONS **485** CITATIONS

SEE PROFILE

Future NEUROLOGY

REVIEW

Current developments in MRI for assessing rodent models of multiple sclerosis

Othman I Alomair[‡,1,2], Maree T Smith[3,4], Ian M Brereton[1], Graham J Galloway[1] & Nyoman D Kurniawan[*,‡,1]

ABSTRACT: MRI is a key radiological imaging technique that plays an important role in the diagnosis and characterization of heterogeneous multiple sclerosis (MS) lesions. Various MRI methodologies such as conventional T_1/T_2 contrast, contrast agent enhancement, diffusion-weighted imaging, magnetization transfer imaging and susceptibility weighted imaging have been developed to determine the severity of MS pathology, including demyelination/remyelination and brain connectivity impairment from axonal loss. The broad spectrum of MS pathology manifests in diverse patient MRI presentations and affects the accuracy of patient diagnosis. To study specific pathological aspects of the disease, rodent models such as experimental autoimmune encephalomyelitis, virus-induced and toxin-induced demyelination have been developed. This review aims to present key developments in MRI methodology for better characterization of rodent models of MS.

KEYWORDS
• axonal loss • demyelination • diffusion-weighted imaging • experimental autoimmune encephalomyelitis • inflammation • magnetic resonance imaging • magnetization transfer imaging • multiple sclerosis • rodent model of multiple sclerosis • susceptibility-weighted imaging

Multiple sclerosis (MS) can be defined as a chronic inflammatory demyelinating disease of the nervous system [1,2]. Early indications of MS-associated symptoms include loss of balance, fatigue, muscle spasms and dizziness, which can progressively develop to complete immobility [3]. Unlike dementia and Alzheimer's disease (AD), which affect the older population, MS can cause clinical disability in the young adult population [3]. According to the MS Research Australia website [4], 23,000 people in Australia have been diagnosed with MS and 2.5 million globally in recent years [5]. The incidence of the disease increases by 7% annually, with the total cost of healthcare in Australia for MS patients being approximately AU$2 billion dollars.

The major cause of MS remains unresolved, as the exact pathobiological mechanisms are not fully understood [1]. However, multiple factors including genetic, gender, ethnicity and environmental factors have been suggested to increase higher disease susceptibility to MS [6]. For example, the gene *HLA DR2* and/or *DW2* is associated with an increased risk of developing MS in the European Caucasian population [7], with a higher incidence of *HLA-DRB1*15*-positive genotypes being reported in female patients [8].

MS is considered as an inflammatory demyelinating disease resulting in disruptions of nerve conduction and neurotransmission [2]. The disease initiates with inflammation and damage to the myelin structure, which normally provides protection and conductivity for the axons of the brain and spinal cord. Once myelin is destroyed, it is replaced by hardened sclerotic patches of tissue, known as sclerotic plaques [1].

[1]Centre for Advanced Imaging, University of Queensland, Brisbane, Queensland, Australia
[2]College of Applied Medical Science, King Saud University, Riyadh, Saudi Arabia
[3]School of Pharmacy, The University of Queensland, Brisbane, Queensland, Australia
[4]Centre for Integrated Preclinical Drug Development, The University of Queensland, Brisbane, Queensland, Australia
*Author for correspondence: n.kurniawan@uq.edu.au
‡Authors contributed equally

Future Medicine part of fsg

Using MRI, MS plaques are commonly observed in various areas of the brain, but the most affected area is the white matter (WM). Highly susceptible areas are the optic nerves, periventricular area, corpus callosum, cerebral peduncle and spinal cord [9]. According to several post-mortem studies [10] and recent MRI studies [11], MS lesions are also present in gray matter (GM). Cortical lesions [12,13] have been detected by ultra-high field MRI (>3 T) [14] utilizing a phase-sensitive inversion recovery MRI sequence [15].

Conventional MRI contrast weighting methods such as inversion recovery, T_1, T_2 and T_2^* have been used widely to detect MS pathology, however, they are nonspecific in describing the progression of neural degeneration [9]. More advanced MR imaging methods have been developed to address these issues: a combination of ultra-high field scanners ≥7 T for humans [16] and ≥9.4 T for rodents [17] and novel contrast agents such as ultra-small super paramagnetic iron oxides (USPIOs) have enabled better detection of early MS changes in the CNS as well as observation of small lesions within the subcortical layers [18]. Magnetization transfer imaging (MTI) has been developed to probe myelin sheath integrity, especially in conjunction with voxel-based analysis to monitor lesion evolution in patients [19]. Susceptibility-weighted imaging (SWI) is highly sensitive to tissue iron content. This sensitivity has been successfully exploited in detecting the presence of iron-rich macrophages and vascular abnormalities during disease progression [20]. Diffusion-weighted imaging (DWI) techniques have been used for early detection of subtle changes in WMs and GMs that appear normal in T_1 and T_2-weighted scans, while diffusion tensor imaging (DTI) fiber tractography can reveal deficits in brain connectivity [21]. DWI methodology is becoming increasingly important as diffusion parameters, fractional anisotropy (FA) and axial/radial diffusivity measures are central to the assessment of MS pathology due to their specificity in detecting demyelination, axonal damage and injury [22].

Animal models of MS

Experimental animal models provide insight into the pathobiology of complex human diseases without replicating the full spectrum of the disease [23]. Animal models are useful to dissect inter-relationships of various factors that contribute to complex pathobiological changes, such as inflammation, demyelination/remyelination and neurodegeneration and their impacts in MS progression/recovery [24]. The commonly used rodent models of MS and their clinical features are summarized in **Table 1**.

• Experimental autoimmune encephalomyelitis

Since its introduction by Rivers *et al.* in 1930 [29], experimental autoimmune encephalomyelitis (EAE) has become a widely used animal model of MS to study acute and chronic axonal injuries. EAE is induced by an injection of an emulsion comprising an adjuvant and synthetic peptides derived from myelin proteins, such as MOG, myelin basic protein or PLP. Alternatively, EAE mice can be prepared using T-cell transfer from EAE donors to native recipients without immunization [30]. In most cases, EAE immunization results in inflammatory activation and expansion of peripheral antigen-specific T cells, which can penetrate the blood–brain barrier (BBB) and promote the demyelination process [25].

There are three types of adjuvants that are used to induce EAE: complete Freud's adjuvant (CFA), pertussis toxin (PT) and the recently introduced Quil A saponin-based adjuvant. A chronic EAE model is induced by injection of $MOG_{35–55}$ with CFA, which slowly releases the antigen from the injection site. The role of PT is unclear, but it is thought to help the initiation of EAE by opening the BBB allowing the migration of immune cells into the CNS. PT is required to initiate T-cell and B-cell immune reactivity to the antigen but it does not, by itself, produce EAE. The acute phase of EAE induction is associated with mononuclear cell infiltration into the CNS, followed by a recovery (remission) period or progressively relapsing in the chronic stage **(Figure 1)**. Clinical scores for rodent models of MS commonly use a scale from 0 to 4, which correspond with no clinical symptoms to severe or flaccid limb paralysis [31].

The limitation of EAE rodent models is that they do not adequately mimic the immonopathology of MS in human patients [25]. $CD4^+$ T cells predominate in EAE CNS lesions [32] but without the predominance of $CD8^+$ T cells and macrophages, which are found in human MS lesions [33]. Nevertheless, various EAE rodent models of MS have increased collectively understanding of the immunopathology aspects of MS. This approach led to US FDA approval of MS therapeutic drugs including glatiramer acetate, mitoxantrone and natalizumab [25].

Table 1. Summary of the type and clinical features of rodent models of multiple sclerosis.

Animal models of MS	Method of induction	Clinical significance and severity	Ref.
EAE	MOG_{35-55} + CFA	Chronic relapsing course without recovery	[25]
Virus-induced demyelination	TMEV	Monophasic stage (relapsing for 7 days and recover within 3 weeks) or biphasic (monophasic with chronic demyelination)	[26]
Toxin-induced demyelination	Cuprizone	Acute or chronic demyelination during the cuprizone diet followed by remyelination	[27]
Toxin-induced demyelination	Lysolecithin	Acute demyelination followed by remyelination	[28]

CFA: Complete Freud's adjuvant; EAE: Experimental autoimmune encephalomyelitis; MS: Multiple sclerosis; TMEV: Theiler's murine encephalomyelitis virus.

• Virus-induced demyelination model

The common virus-induced demyelination model is the Theiler's murine encephalomyelitis virus (TMEV). TMEV is induced by an intracerebral injection of TMEV into susceptible mouse strains, whereby its pathology is limited to the CNS with extensive spinal cord lesion loads [34]. In most cases, TMEV produces chronic progressive MS, which mirrors chronic progressive MS in humans, allowing a closer modeling of the immune response and investigation of the role of viral infection in the etiology of MS [26]. An example of successful application of the TMEV model is the development of anti-glatiramer acetate antibodies as a remyelination agent [35].

• Toxin-induced demyelination model

Lysolecithin and cuprizone are toxins used to investigate the process of demyelination and

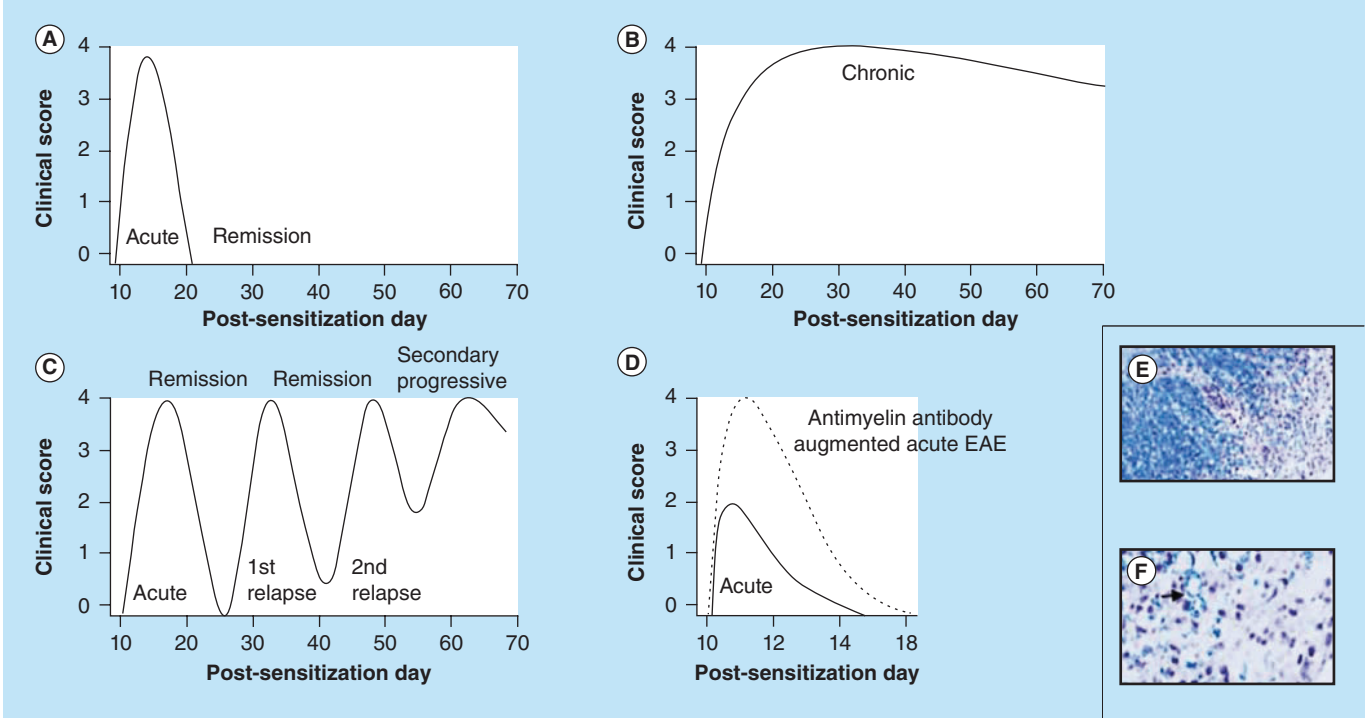

Figure 1. The clinical course spectrum of experimental autoimmune encephalomyelitis mouse models. Immunization of mice with myelin antigens produced an EAE cycle with a characteristic time-dependent pattern of disease severity. **(A)** Acute EAE followed by remission, **(B)** chronic EAE without recovery, **(C)** relapsing–remitting EAE where animals developed relapses and remissions with accumulated neurological deficits. Note that the authors measured the clinical scores based on the paralysis of the hind limbs. **(D)** Adding antimyelin antibodies at 10 days post-EAE immunization results in exacerbated clinical scores (dotted line). Luxol fast blue histology revealed increased axonal damage as well as myelin loss **(F)** compared with control animals **(E)**. The black arrow points to remnants of myelin [31].
EAE: Experimental autoimmune encephalomyelitis.

remyelination of axons [27]. Lysolecithin is an activator of phospholipase, which acts as a detergent on the myelin sheath [25]. Small injections of lysolecithin into the spinal cord produce acute demyelination with the presence of infiltrating T cells, B cells and macrophages. In this model, T cells appear essential for remyelination [28].

Cuprizone is a copper chelator used to induce copper deficits for disruption of oligodendrocyte mitochondrial function and results in demyelination [27]. The addition of 0.2% cuprizone in the diet of young adult mice for 4–5 weeks (acute) or 12 weeks (chronic) will produce focal demyelinated lesions in WM structures, including the corpus callosum, internal capsule, cerebral peduncles, anterior commissure and thalamic WM [27]. Once the cuprizone is removed from the diet, the mice will progressively develop remyelination within 3–4 weeks. Toxin-induced demyelination models are highly reproducible and hence they are useful for testing novel therapeutic approaches for suppressing demyelination and accelerating remyelination processes [25].

MRI studies of animal models of MS

MS clinical studies require recruitment of large numbers of patients with long follow-up procedures and grouping of patients into relevant MS stages. Animal models of MS [24,31] provide better accessibility, allowing monitoring of the environment as well as validation of *in vivo* MRI results using *ex vivo* histology, which is more difficult to achieve in human studies.

In vivo MRI is preferred in MS research as it is noninvasive, facilitates longitudinal studies [36] and enables correlative analysis of various MRI parameters with the status of neurological impairment [37]. On the other hand, *ex vivo* imaging is useful to provide higher resolution without experiment time restrictions increasing the sensitivity of detection of more subtle changes [38]. **Table 2** summarizes MRI observations that are similarly observed in both patients with MS as well as rodent models of MS. In **Table 3**, the underlying pathologies, which cause changes in MRI signals in MS, have been summarized. The typical parameters used in MRI studies of using rodent models of MS are summarized in **Table 4**.

• Conventional MRI

The MRI protocol for assessing MS patients often includes pre- and post-contrast T_1-weighted imaging (T_1 WI), T_2-weighted imaging (T_2 WI) and fluid attenuated inversion

Table 2. Correlation between MRI observations in patients with multiple sclerosis and rodent models.

MRI observations	Human MS studies	Rodent MS studies
T_1WI hypointensity lesions	Detection of advanced MS lesions and tissue damage [39]	Detected in the TMEV mouse model to investigate the role of the adaptive immune system [37]
T_2WI hypointensity lesions in the deep GM	Correlation with clinical disabilities [40] Requires detection using a high magnetic field, such that it may be difficult to apply in the clinical setting	Observed in the TMEV mouse model and could be useful for efficacy assessment of novel MS treatments [41]
Changes in brain volumes	Distinct biomarker for advanced disease progression [42–44]	In EAE mouse model, the loss of cortical volume was due to loss of Purkinje cells in the molecular cortex [45,46]
USPIO enhancement	An indicator of immune cell infiltration and inflammation [47]	Observed in the relapsing remitting EAE mouse model of MS; linked with presence of macrophages and demyelination [48]
Central veins observed on T_2* WI and hypointensity on SWI	Distinctive markers in distinguishing demyelinating from nondemyelinating MS lesions [49]	Similar type of lesions were observed in the lumbar spinal cord and cerebellum of chronic EAE mice [50]

EAE: Experimental autoimmune encephalomyelitis; GM: Gray matter; MS: Multiple sclerosis; SWI: Susceptibility weighted imaging; TMEV: Theiler's murine encephalomyelitis virus; USPIO: Ultra-small super paramagnetic iron oxide; WI: Weighted imaging.

Table 3. Summary of MRI observations and pathological correlations.

Technique	MRI changes in patients with MS	Pathobiological correlations	Ref.	
			Human study	*Animal study*
T_1WI	Hypointensity	Severity of tissue damage	[51]	[37]
T_2WI	Hyperintensity	Active (developing) MS lesions	[39]	[52]
T_1 pre-/post-contrast	Hypointensity	Combination of demyelination and axonal loss	[9]	[52]
T_1 postcontrast	Hyperintensity	Permeability of the BBB and activity of MS lesions	[47]	[52]
MD	Increase	Extracellular edema and inflammation	[53]	[54]
FA	Decrease	Lower axonal bundle coherence in WM lesions or lesions in NAWM	[55,56]	[57]
Axial diffusivity	Decrease	Axonal damage	[58]	[59,60]
Radial diffusivity	Increase	Demyelination		
MTR	Decrease	Progressive demyelination over time	[19,61,62]	[17]
	Recover	Partial remyelination within active MS lesion		
SWI	Hypointense lesions on SWI images	Distinguishing biomarker of active and chronic MS lesions	[63]	[50]

BBB: Blood–brain barrier; FA: Fractional anisotropy; MD: Mean diffusivity; MS: Multiple sclerosis; MTR: Magnetization transfer ratio; NAWM: Normal-appearing white matter; SWI: Susceptibility weighted imaging; WI: Weighted imaging; WM: White matter.

recovery (FLAIR). The most common contrast agents used in MRI are complexes of Gd^{3+}, which is paramagnetic and shortens both T_1 and T_2 relaxation times. These contrast agents stay within the vasculature, unless there is a defect, and do not cross the BBB. At higher magnetic field (≥3 T), Double inversion recovery (DIR) has recently been developed to increase the sensitivity for detecting cortical lesions [11]. These structural MR imaging techniques have played an important role in the study of spatial and temporal characteristics of the disease progression [9,67].

T_1-weighted MRI

T_1-weighted imaging in MS patients

In precontrast T_1 weighted imaging (WI), MS plaques appear hypointense, which is a characteristic of neuronal tissue damage. However, precontrast T_1 WI cannot distinguish the heterogeneous nature of the lesions. Lesions that appear hypointense in pre- and post-contrast T_1 WI are thought to be associated with more severe MS tissue damage exhibiting both demyelination and axonal loss. Postcontrast T_1 WI provides the benefit of measuring BBB permeability, where leakage has been linked to MS lesions and the progression of relapsing symptoms [39].

T_1-weighted imaging in MS animal models

Similar approaches have been used to study MS animal models, including 2D/3D pre- and post-contrast T_1 WI. T_1 WI has been shown to be sensitive to monitor chronic progression in the TMEV mouse model using normal C57BL6 mice and immune differentiation marker-deficient mice [37]. In this experiment, TMEV was administered to four groups of mice, *viz.*: normal C57BL6 mice, as a reference of T_1 hypointensity lesion load; immunodeficient C57BL6 mice RAG-1 deficient; RAG-1-deficient mice with $CD4^+$ and RAG-1-deficient mice with $CD8^+$ T cells. T_1 WI was performed at 7 T to study TMEV lesions. In control C57BL6 mice, T_1 hypointense regions were mostly located in the periventricular area and hippocampus **(Figure 2)**. In RAG-1-deficient mice, there was a significant reduction in the T_1 hypointensity lesion load compared with C57BL6 TMEV mice, indicating the importance of the innate immune system for disease progression. T_1 hypointense lesions increased in RAG-1 mice administered $CD8^+$

Table 4. Typical MRI parameters for imaging animal models of multiple sclerosis.

MRI acquisition parameters and analysis	MS model	Ref.
2D* in vivo *imaging at 9.4 T		
Quantitative T_2: MSME sequence, 16 echoes (TE = 10–160 ms), TR = 300 ms, NEX = 2, in-plane resolution 86 × 86 μm², 1-mm slice thickness MTR: two SE images with and without off-resonance pulses, TR/TE = 3000/10 ms, 2 KHz off-resonance pulse, NEX = 2, in-plane resolution 86 × 86 μm², 1-mm slice thickness DTI: DWI spin-echo EPI, TR/TE = 3000/25 ms, Δ/δ = 10/4.5 ms, four EPI segments, 1 b0, 15 diffusion encoding gradients, b = 1000 s/mm², 150 × 150 μm², 1-mm slice thickness Data analysis based on whole-brain histogram and VBA	Chronic EAE in C57BL6 mice. Relapsing–remitting EAE in SJL mice	[17]
3D* in vivo *imaging at 7 T		
T_1 WI: gradient echo FLASH sequence, TR/TE = 15/4.5 ms, NEX = 2, with 125 × 150 × 150 μm³ resolution T_2 WI: FSE sequence, TR/TE = 1500/70 ms, RARE factor 16, with 125 × 150 × 150 μm³ resolution Brain structure (ventricular volume) was measured using semiautomated tracing method	TMEV-induced chronic progressive demyelination in SJL mice	[64]
3D* in vivo *imaging at 7 T		
T_2 WI: MSME sequence, TR/TE = 5741/50 ms, eight echoes, NEX = 16, 150 μm³ isotropic resolution 3D *ex vivo* imaging at 7 T T_2 WI: FSE sequence, TR/TE = 5741/50 ms, ETL factor = 8, NEX = 80, with 64 μm³ resolution Semiautomated skull stripping using BrainSuite2, image registration using Automated Image Registration, and processing using LONI Pipeline Processing Environment	Chronic EAE by CFA + PTX immunization in C57BL6 mice	[46]
2D* in vivo *imaging at 4.7 T		
DTI: DWI spin echo sequence resolution, TR/TE = 1500/50 ms, Δ/δ = 25/8 ms, six diffusion encoding directions, NEX = 4, in-plane resolution 59 × 59 μm², 1-mm slice thickness, 3-h acquisition AD, RD and RA maps were analyzed using ROI-based analysis	Cuprizone-induced demyelination in C57BL6	[65]
3D* in vivo *imaging of cerebellum & lumber spinal cord at 9.4 T		
SWI: GEFC TR/TE = 4/50 ms, NEX = 17, resolution 48 × 100 × 400 μm³, coronal slices for cerebellum and axial slices for lumber spinal cord. The mice were imaged at 16–19 days, in addition to long-term 30 days and 6 months postimmunization	Chronic EAE induced in C57BL6 by MOG + CFA + PTX	[50]
2D* in vivo *of the brain & upper spinal cord at 1.5 T		
Detection of USPIO/macrophages: coronal T_2 WI FSE, TR/TE= 1437/100 ms, coronal T_1 SE, TR/TE = 500/10 ms, with in-plane resolution = 58.6 × 58.6 μm², slice thickness = 3000 μm The mice were imaged 9.2 ± 2.8 days postimmunization after the first attack and another group imaged again during the second attack 17.9 ± 4.4 postimmunization	Relapsing–remitting EAE induced in DA rats using emulsion comprises spinal cord + IFA	[48]
3D* in vivo *imaging at 7 T		
Detection of BBB leakage: pre- and post-Gd contrast T_1 WI SE TR/TE= 150/8 ms, NEX = 1, resolution = 200 × 200 × 200 μm³ BBB leakage volumes were generated using semiautomatic method based on combination of threshold and seed growing tool	Assessing vascular permeability using combination of PIFS and TMEV models	[66]

AD: Axial diffusivity; BBB: Blood–brain barrier; CFA: Complete Freud's adjuvant; DA: Dark Agouti; DTI: Diffusion tensor imaging; DWI: Diffusion-weighted imaging; EAE: Experimental autoimmune encephalomyelitis; EPI: Echo Planar Imaging; ETL: Echo train length; FLASH: Fast low-angle shot; FSE: Fast spin echo; GEFC: Gradient echo flow compensated; IFA: Incomplete Freud's adjuvant; LONI: Laboratory of Neuroimaging; MS: Multiple sclerosis; MSME: Multislice multiecho; MTR: Magnetization transfer ratio; NEX: Number of excitations; PIFS: Peptide-induced fatal syndrome; PTX: Pertussis toxin; RA: Rheumatoid arthritis; RARE: Rapid acquisition with relaxation enhancement; RD: Radial diffusivity; ROI: Region of interest; SE: Spin echo; SJL: Swiss Webster mice from the Jackson Laboratory; SWI: Susceptibility weighted imaging; TE: Echo time; TMEV: Theiler's murine encephalomyelitis virus; TR: Repetition time; USPIO: Ultra-small super paramagnetic iron oxide; VBA: Voxel-based analysis; WI: Weighted imaging.

T cells, but were unaffected in RAG-1 mice administered $CD4^+$ T cells.

Lesions with strong T_1 hypointensity (also referred to as T_1 black holes) were suggested to represent areas of severe tissue damage with axonal and neuronal loss, and helped to distinguish the significance of different types of T cells in mediating brain damage. This study further highlights the distinctive role of $CD4^+$ T cells (or T helper cells), which play a major role in the EAE model [26,68]; compared with the role of $CD8^+$ cells in the TMEV mouse model of MS. It has been suggested that these differences may have contributed to the lack of

success of treatments targeting $CD4^+$ T cells in the treatment of human MS [37].

T_2-weighted MRI

T_2-weighted imaging in MS patients

T_2 WI plays a major role in the detection of MS lesions. The detection of new T_2 hyperintense lesions after the onset of the first MS attack signifies further progression of the disease, and indicates the beginning of the relapsing remitting disease course [67]. High-resolution T_2 WI has also been used to detect brain atrophy in patients with MS [42].

On one hand, T_2 hypointensity may be caused by several factors including iron, free radicals, the presence of macrophages and deoxyhemoglobin [69]. T_2 hypointensity has been reported in human studies, but as the lesions were located within the deep GM, biopsies were difficult to perform to investigate the tissue properties [69]. In a human MS study at 3 T [70], there was a correlation between the physical changes assessed using the expanded disability status scale (EDSS) and alterations of signal intensities in the globus pallidus and caudate nucleus ($r = -0.5$; $p < 0.05$). In a separate study, iron deposition in deep GM structures has been assessed by T_2 hypointensity and was shown to have some correlation with neuropsychological score of cognitive dysfunction (Pearson's correlation between T_2 hypointensity and neuropsychological score has the range between $r = 0.265$ and 0.395) [71].

On the other hand, T_2 hyperintensity may serve as a potential biomarker for detecting active MS lesions [9] but with low specificity to acute and chronic MS disease pathology [72]. This is due to the presence of inflammation, edema and demyelination in acute lesions, and profound demyelination, axonal loss and gliosis in chronic lesions [9], which could result in the elevation of tissue water content and consequently lead to indistinguishable causes of T_2 hyperintensity [73]. A 20-year follow-up study with more than 100 patients [67], showed that T_2 lesion volume at multiple time-points (0, 1, 5, 10, 14 and 20 years) correlated moderately to EDSS ($r_s = 0.48$ to 0.67; $p < 0.001$) and to MS functional composite z-score ($r_s = -0.50$ to -0.61; $p < 0.001$). The rate of volume increase in T_2 lesions is three-times higher in the patients who develop secondary progressive compared with the patients who remain relapsing–emitting.

T_2-weighted imaging in MS animal models

High-resolution T_2 WI has been shown to be useful for measurement of volumetric changes in EAE mouse brains and can be correlated with histopathological analysis [45]. This *ex vivo* MRI study in EAE mice found significant reductions in the volume of the cerebellum, cerebellar cortex and molecular layer of the cerebellar cortex. Atrophy in the molecular layer of the cerebellar cortex is related to loss of Purkinje cells [74]. Such detection of GM atrophy was important as it was correlated with progressive development of clinical disability ($r = -0.6207$; $n = 21$; $p = 0.0027$) [45,75].

Brain atrophy is known as MS human pathology [1] and this has been observed in TMEV model. Using serial 3D T_1 WI and T_2 WI of a TMEV SJL/J mice from 0 to 12 months post immunization, significant atrophy was observed in affected mice at 3 months and reaches its peak by 6 months with 118% increase in the ventricular size. However, it is still not understood how deep TMEV GM lesions contribute to the observed atrophy [64]. A more recent T_2 WI *in vivo* study in EAE mice from the same group [46] re-affirmed the presence of GM atrophy in the cerebral cortex, characterized by a major decrease in the volume of the cerebellum by 80 days post-EAE induction [46]. However, there was no discernable correlation between disease severity and whole brain volume, or volume changes in the cerebral cortices during the course of the disease. Detailed volumetric analyses of various brain regions in C57 BL6 mice may benefit from recent high-resolution C57 BL6 brain atlas acquired at 16.4 T [76].

T_2 WI hypointense regions have been detected in the deep GM structures of TMEV SJL/J mice, in the thalamus, caudate, putamen and dentate nuclei **(Figure 3)**. The gradual development of T_2 hypointensity intensity thalamic lesions appeared to be correlated with progressive rotarod detectable disability ($p < 0.001$) [41]. It was suggested that the hypointensity is due to the presence of extravasated blood in this area.

Correlation of T_1- and T_2-weighted signal intensity with histopathology requires animal models that can produce a large number of inflammatory lesions. This has been established in a T-cell clonal adaptive transfer EAE model using SJL/J mice, in which the lesion formation was traced using 3D high-resolution T_1 WI and T_2 WI at 2.35 T [52]. During the acute stage (9 days postadaptive transfer), two independent

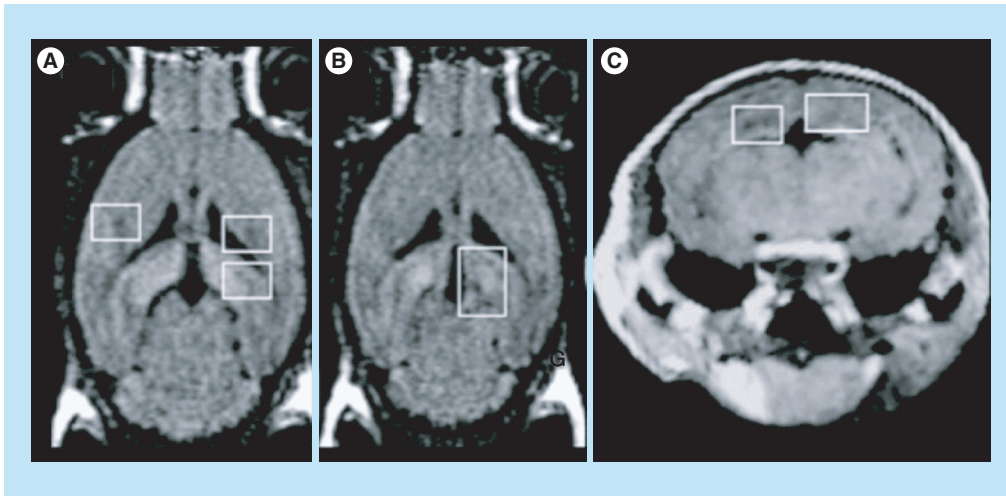

Figure 2. 3D T_1-weighted imaging at 7 T of C57BL6 infected with Theiler's murine encephalomyelitis virus. Coronal **(A, B)** and axial **(C)** sections were extracted from 3D T_1 WI 7 days postinfection. T_1 hypointense lesions were more pronounced in the periventricular area and adjacent to the hippocampus as indicated by the white frames. (TR/TE= 200/10 ms, voxel dimensions = 135 × 200 × 200 μm^3) [37].
TE: Echo time; TR: Repetition time

patterns of lesions were detected: hypointense lesions on both T_1 and T_2 WI (type A lesions), other lesions, characterized by slightly hypointese or isointense T_1 WI and hyperintensity on T_2 WI (type B lesions). Histology studies showed that type A lesions contained a higher density of inflammatory cells and myelin loss and they were more destructive than type B lesions. Serial MRI was performed during the disease cycle, and the patterns of two lesions were heterogeneous. At the end of the disease cycle (30 days postadaptive transfer), for type A lesions, T_1 hypointensity persisted and T_2 hypointensity diminished (returned to isointensity). For type B lesions, T_1 hypointensity diminished and T_2 hyperintensity persisted.

This experiment also revealed high correlations between T_1 and T_2 signal intensity with cellular parameters of inflamatory tissue damage [52]. The density of activated microglia cells, reactive astrocytes and immunoglobin deposition was positively correlated with the signal intensities of the T_2 WI (with the corrlation r = 0.62–0.73; $p < 0.04$). However, the signal intensities of T_1 WI have negative correlations with microgila cell densities and astrocytes (r = -0.67; $p < 0.02$).

Inversion recovery MRI

Inversion recovery applications in MS patients

DIR and FLAIR imaging can increase the sensitivity of detecting focal areas of hyperintensity, especially in GM and cortical lesions by suppressing either the WM, GM or cerebrospinal fluid (CSF) signals [13,77]. However, these techniques have low sensitivity for the heterogeneous pathologic substrate of individual lesions. FLAIR can detect lesions that are involved in WM structures such as leukocortical or juxtacortical lesions but the vast majority of the intracortical lesions are not detected such as subpial cortical lesions. On the other hand, the DIR sequence comprises double inversion pulses: one to suppress CSF signals and another one to suppress the WM signals. This sequence provides low S/N; however, it offers excellent contrast-to-noise ratio, which facilitates detection of more MS lesions in GM [10]. A recent post-mortem MS study carried out on 14 patients assessed the sensitivity and specificity of 3D DIR and 3D FLAIR. 3D DIR was more sensitive and specific by 18 and 90% in the detection of cortical lesions. These findings have been confirmed using PLP myelin stain [10].

A recent study [78] compared T_1 WI, T_2 WI and FLAIR at both 3 T and 7 T, but imaging using these techniques at higher magnetic field did not appear to increase sensitivity for detection of WM lesions. 3D-FLAIR at 7 T has been tailored to improve sensitivity in depicting GM lesions [78]. This technique combined axial FLAIR (1 mm^3 isotropic resolution) and T_2* WI (0.55 mm^3 isotropic resolution), to produce

FLAIR* with 0.55 mm^3 isotropic resolution [77]. The resulting image showed suppression of CSF and high-resolution visualization of microvascular structures, which enabled investigation of the presence of interlesional veins in WM lesions [77]. Such lesions were detected in the pons and cerebellum and were related to the presence of iron-containing macrophages [77].

Inversion recovery applications in MS animal model

In rodent brain MRI, inversion recovery is used to produce a stronger T_1 weighting and CSF suppression. For example, a T_1-weighted 3D modified driven equilibrium Fourier transformation sequence at 9.4 T [79] was used to enhance visualization of cortical areas, the striatum and the ventricular system. However, T_1 WI modified driven equilibrium Fourier transformation could not detect EAE inflammatory lesions, in contrast to T_2 and T_2* WI [79]. FLAIR with inversion recovery does not appear to have been applied to the study of rodent models of MS. Fluid attenuation using FLAIR is not commonly used as the T_1 relaxation time is considerably longer at the high magnetic fields commonly used in animal MRI studies [79].

Limitation of conventional MRI in rodent models of MS

The low specificity of conventional MRI techniques to monitor and characterise MS lesions is due to the heterogeneity of MS lesions, comprising cellular debris from demyelination/remyelination processes, permanent axonal loss, increased immunocellular activity and tissue edema, all of which can affect the T_1 and T_2 contrast [9]. However, T_1- and T_2 WI could not detect MS lesions within normal-appearing WM (NAWM), which was shown to be present in post-mortem studies [80].

Imaging of the rodent brain is challenging due to several technical issues such as subject breathing motion and susceptibility image artifacts from sinus and ear cavities. Respiratory gating, however, is rarely used for brain imaging, except for DWI, as it significantly prolongs the acquisition time. High in-plane resolution (sub

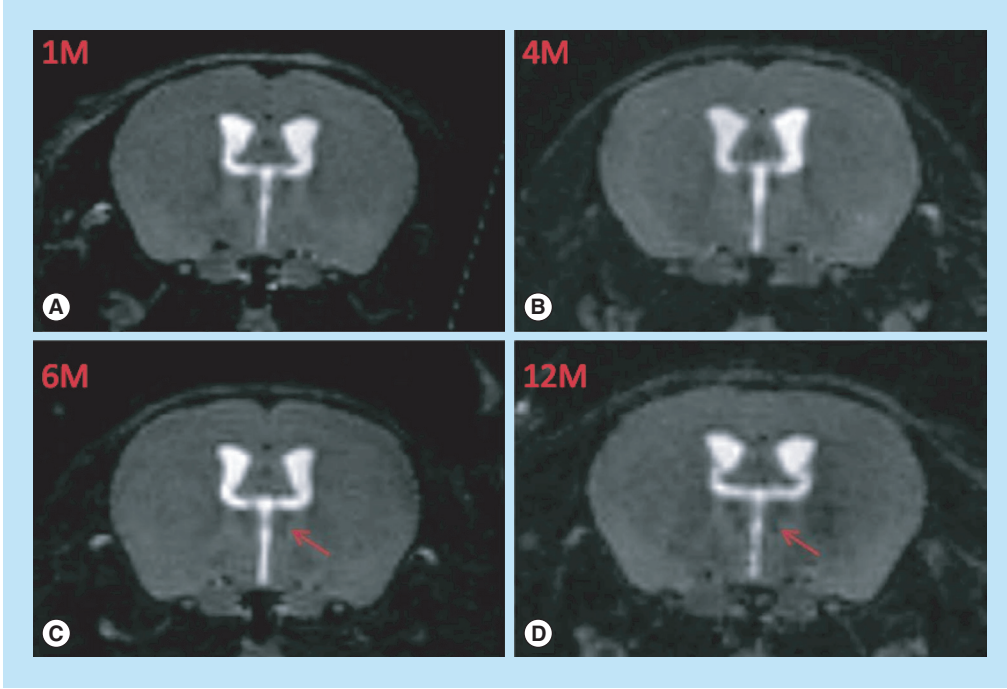

Figure 3. The correlation between increasing hypointensity of the mediodorsal thalamic nucleus on T_2-weighted images and disease progression. (A) 1 month postdisease induction, **(B)** 4 months, **(C)** 6 months and **(D)** 12 months as indicated by red arrows. 3D volume RARE sequence at 7 T with TR = 1500 ms, TE = 70 ms, ETL = 16, FOV = 3.20 × 1.92 × 1.92 cm, voxel dimensions = 125 × 150 × 150 μm^3 [41].
ETL: Echo train length; FOV: Field of view; RARE: Rapid acquisition with relaxation enhancement; TE: Echo time; TR: Relaxation time.

100 μm^2) with relatively thicker slices (1 mm) are often used to provide sufficient resolution to distinguish small structures in the rodent brain at the expense of partial volume effects [81]. The acquisition of 3D isotropic dataset at medium resolution (>125 μm^3) can be accomplished but this will increase the acquisition time and is more sensitive to motion [36]. For high-resolution rodent brain imaging, high magnetic fields (>7 T) are typically used to boost S/N, but suffer from higher local magnetic field susceptibility and longer T_1 and shorter T_2 relaxation times. In live imaging, acquisition parameters should be optimized to acquire high S/N and resolution within the shortest experiment time [81].

Cryogenic radiofrequency coil mouse brain MRI

The recent introduction of cryogenically cooled radio frequency (RF) coils (cryocoil) may improve the role of conventional micro MRI in assessing pathological changes in rodent models. At 9.4 T, cryogenic coils boost S/N by a factor of up to 2.9, which can be exploited to significantly shorten experiment time for *in vivo* imaging [82,83]. For example, a volumetric T_2 WI at (60 μm^3) isotropic resolution could be acquired within 45 min. The cryocoil has a maximum signal penetration of approximately 3 mm from the brain surface and can reveal intricate cortical and subcortical details of the mouse brain [83]. Despite its high sensitivity, the cryocoil has some disadvantages in terms of its inhomogeneous RF excitation profile. Gradual loss of S/N for deeper (ventral) brain structures was also observed due to the positioning of the surface array coil on the cortex. However, such artifacts can be minimized with careful adjustment of the RF power and image postprocessing [82,83].

In vivo conventional micro MRI using the cryocoil (T_1, T_2 and T_2* weighted imaging) has been used to detect MS lesions prior to the appearance of the symptoms in EAE mice immunized with $PLP_{139–151}$ [79]. High-resolution images T_1 WI, T_2 WI (47 × 47 × 400 μm^3) and T_2* WI (35 × 35 × 400 μm^3) were used to detect MS lesions in the cerebellum, cerebral cortex and subcortical region before the disease manifestations **(Figure 4)** [79].

• Contrast agent enhancement & cellular tracking

Paramagnetic gadolinium (Gd) contrast agents and ultra-small and small superparamagnetic iron oxide (USPIO and SPIO) particles are commonly used to investigate MS. These compounds produced distinctive contrast by shortening the T_1 and T_2 relaxations of the surrounding tissue. Due to their specific relaxivity, Gd-DTPA is often used for T_1 WI as hyperintensity, whereas USPIO/SPIO with T_2 or T_2* WI as hypointensity [39].

USPIO & SPIO particles

USPIO and SPIO particles [39] have been used to monitor the cellular mechanisms of MS inflammation. The cells of the monocyte-macrophage system take up the iron oxide particles and their infiltration into the lesion sites could be detected using MRI using T_2* WI [84]. Several studies [18,47] have shown that the USPIO pattern of enhancements is correlated with MS disability, axonal loss and patient's response to treatment.

The biological specificity of the USPIO depends upon the molecular characteristics of the applied particles [18]. For example, USPIO particles SHU555C and Ferumoxtran-10 differ in size (25 vs 30 nm), and body circulation half-life (6–8 h vs 24–30 h). *In vitro*, the negative charge on SHU555C particles produced preferential uptake by activated monocytes [85].

USPIOs have been used as indicator of disease progression in rats with relapsing–remitting (RR) EAE [48]. Rats with positive detection of USPIO particles (+USPIO rats) show significant tissue alteration at the first attack and more severe clinical signs compared to -USPIO rats during the second attack **(Figure 5)**. This study demonstrates how USPIOs can be used to determine the role of macrophage infiltration as an indicator of progressing inflammatory demyelination.

Gd-contrast agent

Gd T_1 WI postcontrast studies have been used to monitor BBB permeability which can be disrupted during deposition of new MS lesions [66,86]. In one study, Gd T_1 WI postcontrast was used to determine the role of CD8 T cells and neutrophils in causing BBB permeability, using a modified model of C57/BL6 TMEV mice exhibiting peptide-induced fatal syndrome (PIFS) [66]. Gd T_1 WI postcontrast showed that the ablation of immune cells using nonspecific anti-GR-1 monoclonal antibody RB6-8C5 (which also ablated CD8 T cells) successfully prevented BBB leakage. However, this was not the case for animals receiving treatments with normal rabbit

serum (NRS) as a negative treatment control, nor animals treated with anti-Ly-6G mAb 1A8 (specific to ablate neutrophils) **(Figure 6)**. The Gd T_1 WI postcontrast data show strong correlation between the prevention of BBB damage and the preservation of motor function, and it helped to determine that the activity of CD8 T cells in damaging BBB was independent of neutrophils activity [66].

There remains controversy as to whether Gd or USPIO provides a better early indication of MS pathology [18]. In some cases, USPIO is superior to Gd, because it can detect lesions a few weeks earlier than Gd enhancement [18]. USPIO lesion enhancement may persist longer after Gd enhancement has ceased and shows spatial distribution of the immune-reactive cells post-BBB repair [39]. A recent comparison between USPIO and Gd enhancements in ten patients with RR-MS [47] showed that the same lesions were seen with both contrast agents, but that some of the lesions were specifically observed by USPIO only or Gd only [47]. Nevertheless, current data indicate that USPIOs and Gd have specific biological pattern of enhancements that are important in characterizing MS. Gadolinium enhancement reflects leakage of the BBB whereas the USPIOs' enhancements represent cellular infiltration [47]. Careful considerations must be given when choosing these contrast agents to take advantage of their specificity.

• DWI & tractography

Introduction to DTI

The measurement of tissue molecular diffusion using DWI is widely used in MS research [53]. MRI is sensitized to microscopic diffusion of water in tissue by the application of diffusion gradients. Gaussian modeling of tissue water diffusion can broadly be classified as nonrestricted (isotropic) and directionally restricted (anisotropic) diffusion. In neuronal tissues, isotropic diffusion can be identified within CSF and to a lesser extent in GM, whereas anisotropic diffusion has often been correlated with the degree of myelination and axonal fiber directionality of the WM [87].

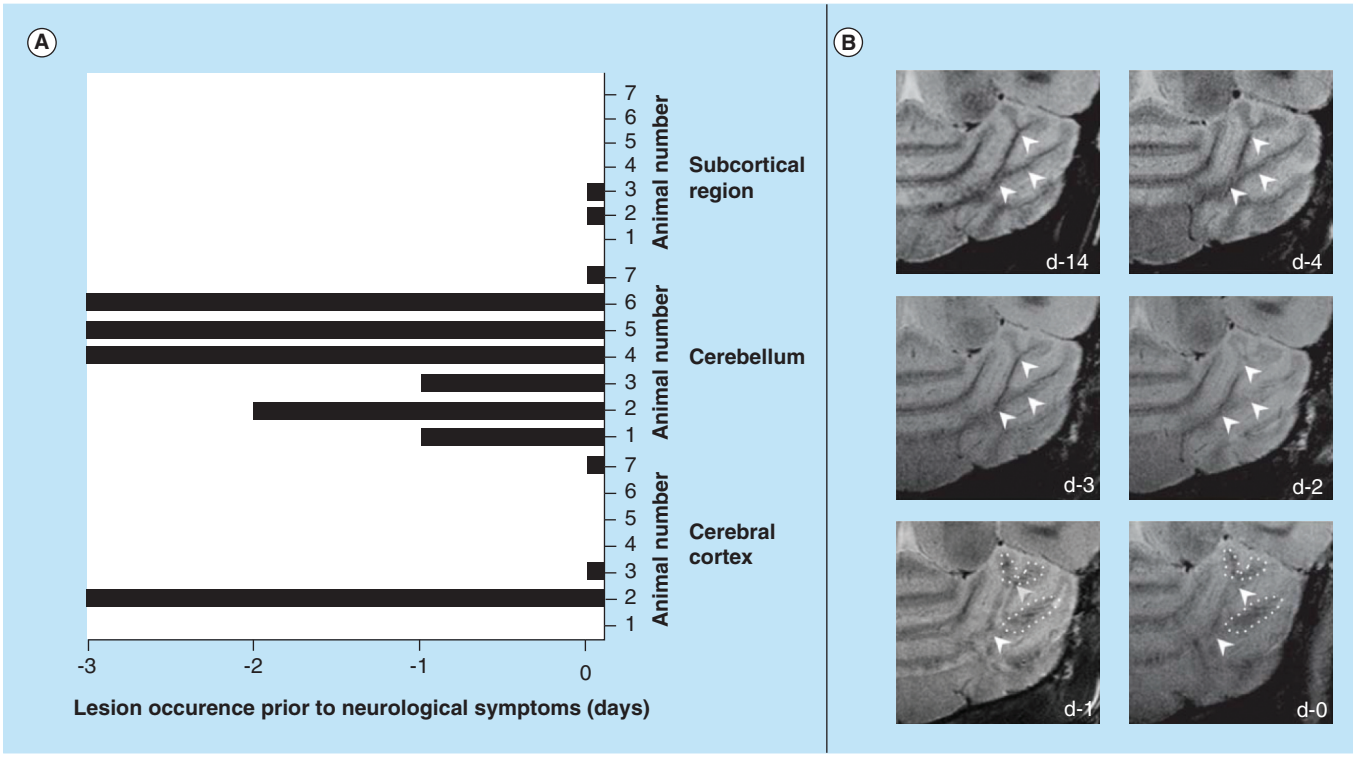

Figure 4. Application of micro MRI T_2-weighted images in assessing evolution of the lesion prior and during disease onset.
(A) Detection of multiple sclerosis lesions in subcortical region, cerebellum and cerebral cortex in seven experimental autoimmune encephalomyelitis mice prior to the disease onset until the disease starting time. **(B)** T_2-weighted images from d-14 prior to disease manifestation until d-0 when symptoms were initiated [79]. Arrowheads show progressive increase of white matter signal intensity over time and dotted areas show disappearance of signals in the surrounding tissue.
d: Day.

The directionality and strength of anisotropic diffusion can generally be described as an ellipsoid diffusion tensor, which can be measured using magnetic resonance DTI [87]. DTI acquisition requires a minimum of six orthogonally encoded DW images and one unweighted image [88]. From these measurements, three eigenvectors (ν_1, ν_2, ν_3) and their rotational invariant eigenvalues (λ_1, λ_2, λ_3) can be derived to describe the diffusion tensor [88]. The largest eigenvector (ν_1), the direction of the major diffusion component and its associated eigenvalue (λ_1) represent the magnitude of axial diffusivity along the length of the axonal fiber bundle [89]. ν_2, λ_2 and ν_3, λ_3 describe transverse diffusion components orthogonal to the fiber bundle, where the average of λ_2 and λ_3 is known as radial diffusivity **(Figure 7)** [89].

DTI parameters can be used to derive rotational invariant diffusion metrics: mean diffusivity (MD), FA and relative anisotropy (RA). MD describes the average of diffusivity components within each voxel [90]. The diffusion tensor parametric FA is more commonly used than RA in the DTI literature [91]. FA values range from 0 to 1 to describe the degree of the anisotropy of the intravoxel diffusivity [92]. FA values in WM are generally higher than in GM due to increased diffusion directionality of the myelin axon bundles [88].

DTI parameter changes in MS patients

DTI-derived parameters are powerful and sensitive measures for assessing MS pathological changes. MS pathology is associated with damage to the WM myelin structure, resulting in disruption of molecular water diffusion and a consequential reduction in diffusion anisotropy [9]. A summary of DTI parametric changes in WM affected by MS is illustrated in **Figure 7**.

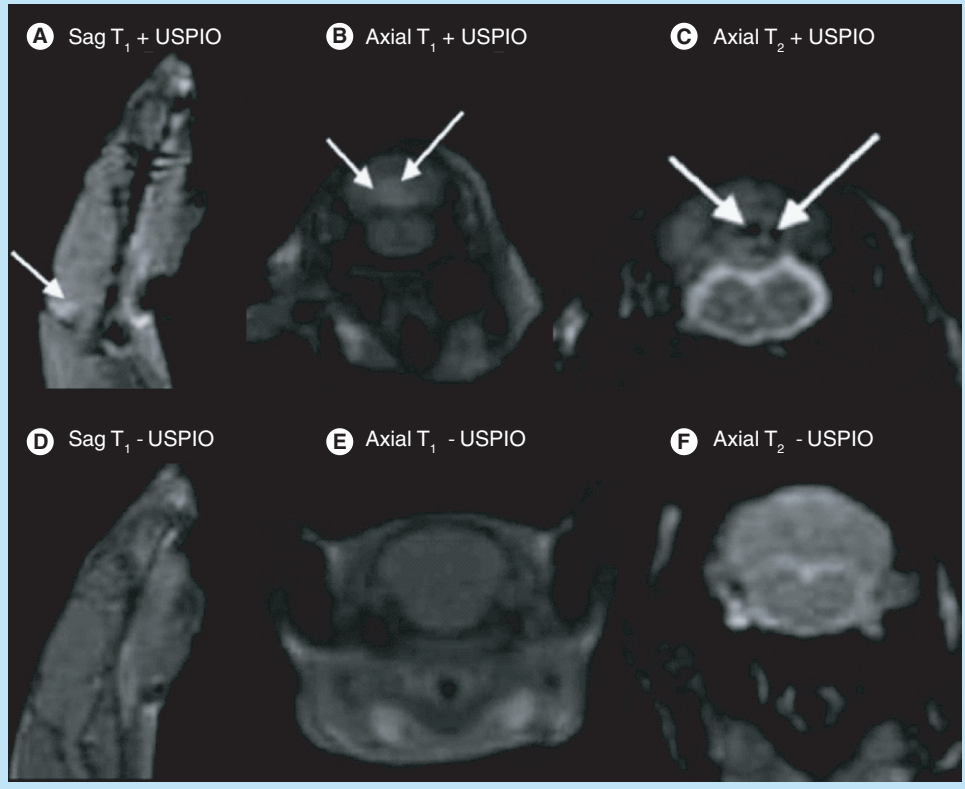

Figure 5. Detection of macrophages using ultra-small super paramagnetic iron oxide contrast agent at 1.5 T for assessment of their role in the development of secondary progressive experimental autoimmune encephalomyelitis in rats. (A) Sagittal T_1 WI and **(B)** axial T_1 WI show hyperintensity and reflect the uptake of USPIOs in the CNS. **(C)** Axial T_2 WI shows hypointensity as indicated by arrows. These signal alterations were not observed **(D)**, **(E)** and **(F)** with other experimental autoimmune encephalomyelitis rats in this experiment [48].
Sag: Sagittal; USPIO: Ultra-small super paramagnetic iron oxide.

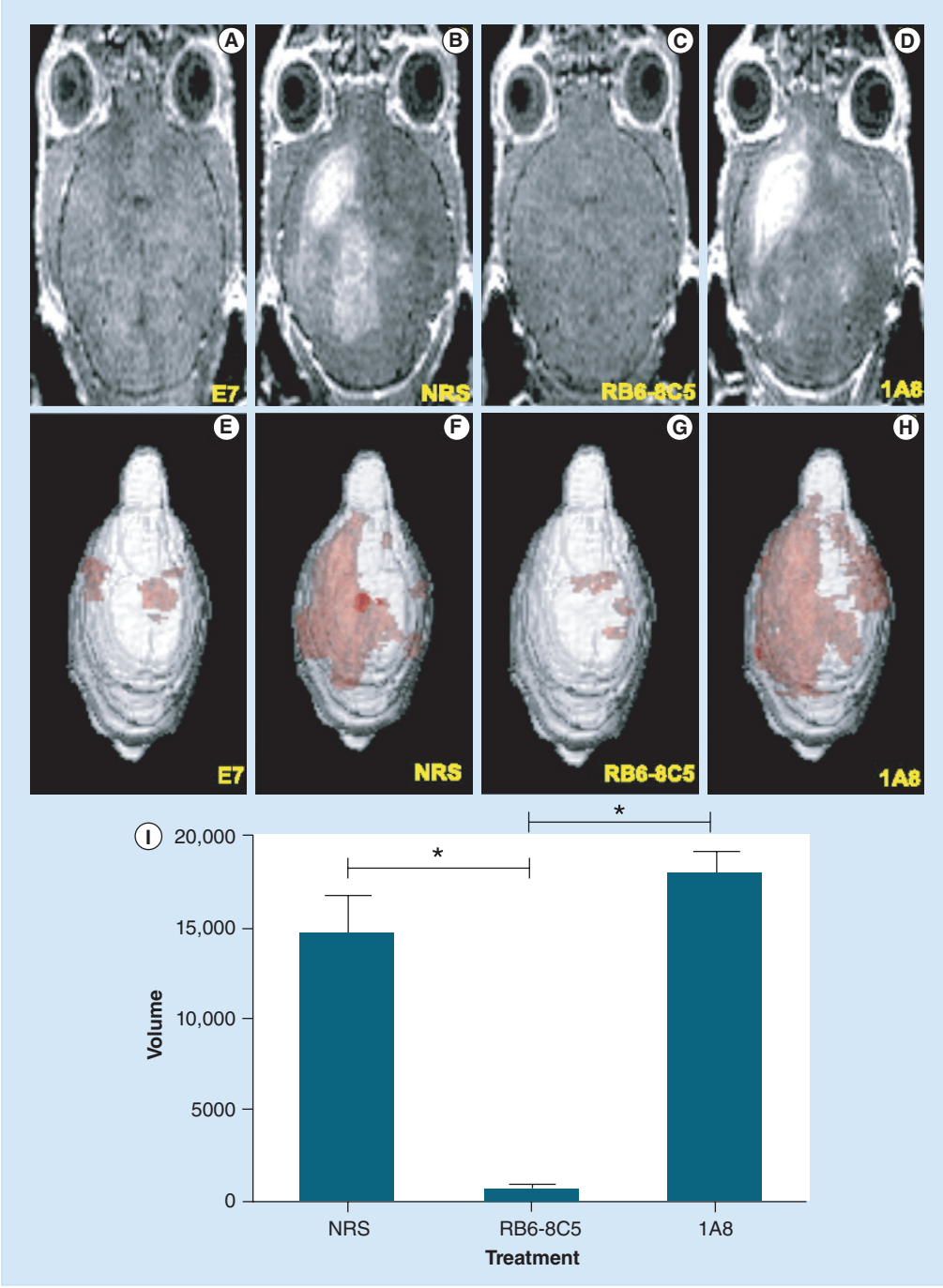

Figure 6. Analysis of the role of CD8 T cells and neutrophils for the initiation of blood–brain barrier disruption in peptide-induced fatal syndrome modified Theiler's murine encephalomyelitis virus model using Gd-enhanced T_1 WI. (A) A 7-day Theiler's murine encephalomyelitis virus mouse without peptide-induced fatal syndrome (control). **(B–D)** C57BL/6 mice undergoing peptide-induced fatal syndrome receiving treatments to deplete neutrophils *in vivo*: **(B)** normal rat serum (as a negative control treatment), **(C)** with nonspecific antibody RB6-8C5 or **(D)** with neutrophil-specific 1A8 antibody. **(E–H)** Red subvolumes are rendering of gadolinium-enhancing areas. **(I)** Quantification of blood–brain barrier permeability areas from each group [66], units = number of voxel (0.008 mm^3 per voxel).
NRS: Normal rabbit serum.

DTI parametric maps provide distinguishing characteristics for careful interpretation of MS lesions, even for those that are readily detectable by the conventional imaging techniques [55]. Compared with the NAWM, MS focal lesions showed increased MD which indicated some loss of the structural barrier to water molecular diffusion and a decrease in FA due to disorganization of WM structures [53]. Co-localization of T_1 hypointense and DTI lesions may signify areas suffering from irreversible tissue damage [93]. Additionally, a longitudinal progressive MS study [94] showed that worsening lesions could be detected more sensitively as areas with increasing MD, which were otherwise indistinguishable using postcontrast T_1 WI. On the other hand, lesion areas with increased T_2 relaxation time and increased MD appear to reflect a decrease in the axonal myelin (intracellular) water content and an increase in the extracellular water due to tissue damage [95].

A recent study [58] has assessed the axial and radial diffusivities within the abnormally low FA areas in the brains of patients with MS. The brain regions examined include fornices, inferior longitudinal fasciculus, optic radiations and parts of the corpus callosum. There was an increase in RD caused by demyelination but surprisingly, there was only a small increase in AD [58]. A complicated pattern of change in diffusivities may occur due to axonal loss [96] or an increase in axonal diameter. This was supported by previous findings in post-mortem MS spinal cord studies which showed areas of T_2 WI hyperintensities [97]. For areas containing crossing fibers, abnormal changes to the FA, AD and RD must be carefully assessed as MS pathology in these areas can produce unexpected results such as an apparent increase in diffusion anisotropy [92].

Many DTI studies of human MS [98,99] and rodent models [54,57] are focused on the WM structures as they are the anticipated sites of MS pathological changes. High WM anisotropy provides characteristics for sensitive detection of MS pathological changes using DTI measures [58,99]. MS, however, is a whole brain disease and can also affect GM and cortical areas [39]. A 3-year longitudinal study of relapsing–remitting MS patients at 1.5 T has reported an increase of FA in normal-appearing GM (NAGM) and cortical lesion volume, which are correlated with clinical disability ($r > 0.75$; $p < 0.01$) [11]. The increase of FA was unexpected, but it was suggested to be associated with a low degree of inflamation, demyelination, axonal damage and neuronal loss in NAGM cortical lesions. The presence of activated microglia could play a strong contribution to this increase of FA, as activated microglia are known to change their shape into a more anisotropic flat bipolar structure, resulting in apparent increase of anisotropy in these lesions [11].

DTI studies of MS animal models

AD and RD measurements are potentially more sensitive than MD in diagnosis of MS lessions due to characteristic high-diffusion anisotropy in the WM [91,100]. In MS studies using the cuprizone rodent model [59,101], decreasing AD and increasing RD were robust surrogate markers for axonal damage and demyelination, respectively. These conditions were observed in various DTI MRI animal studies, for example: in a retinal ischemia mouse model, where a decrease of AD correlated with axonal injury [102]. In a spinal DTI study of a mouse model of chronic EAE [103], histology data confirmed a correlation of intense anti-β-amyloid precursor protein staining with a decrease in AD associated with axonal damage; and an increase in radial diffusivity with diminished luxol fast blue staining as a biomarker of demyelination. In a cuprizone-induced demyelination/remyelination mouse model [54], T_2 hyperintensity, a reduction in AD and an increase in RD were specifically observed in the caudal segment of the corpus callosum, and these were correlated with histological observations of demyelination (luxol fast blue staining), axonal injury (neurofilaments staining), microglial accumulation and cellular infiltration. In inflammatory optic neuritis in an EAE mouse model [104,105], uniform optic neuritis resulted in axonal injury (decreased AD) and demyelination (increased RD), as shown in **Figure 8**.

Investigation of DTI parametric changes in MS rodent models [54,57] may not necessarily translate to detection of pathological changes in patients with MS. For example in the mouse model of MS, changes in RD were not observed, although severe demyelination, inflamation and axonal damage were detected by histology [90]. Such negative observations may be due to confounding factors affecting RD senstivity for detection of demyelination; for example, inflammation due to the presence of activated microglia and macrophages, T-cell infiltration, as well as vasogenic edema affect the apparent diffusion anisotropy in MS lesions [90,106].

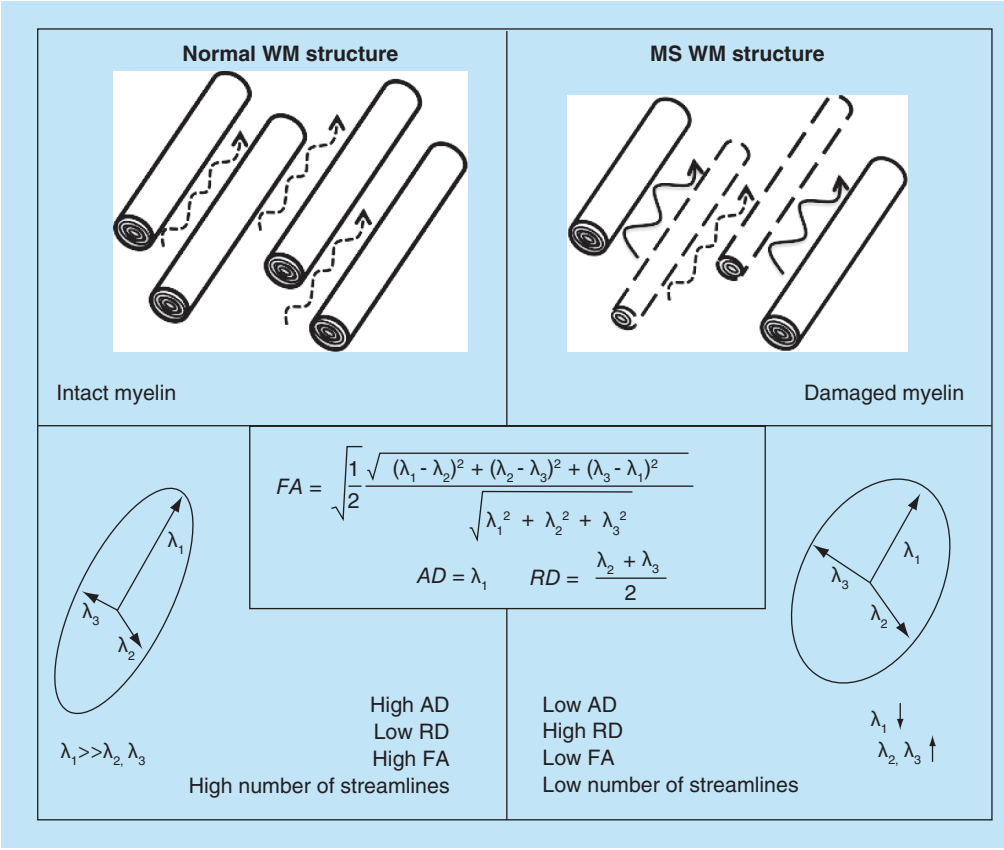

Figure 7. The relationships between the white matter axonal fibers, myelin structure and diffusion tensor imaging derived parameters in multiple sclerosis pathology. The demyelination, axonal injury and inflammation processes in multiple sclerosis typically result in a decrease of FA, and AD and an increase in RD.

AD: Axial diffusivity; FA: Fractional anisotropy; MS: Multiple sclerosis; RD: Radial diffusivity; WM: White matter.

DTI tractography studies in MS patients

DTI tractography reconstruction provides a unique depiction of 3D projections of neural structures, which is useful for studying brain connectivity. DTI tractography can potentially be used to stage MS progression as MS lesions produce local or global disruptions in the WM fiber architecture that affect fiber tractography profiles and streamline numbers [107]. DTI tractography is useful for extracting WM pathways in patients with MS, for example, in the corpus callosum, for investigation of undetected NAWM lesions and consequential correlation between the clinical symptoms and the imaging findings [55,98].

There are various methods available to process DWI data in performing tractography [108]. In general, tractography image processing first involves the determination of fiber orientation distribution, followed by the propagation of tracts (streamlines) using deterministic or probabilistic fiber tracking methods [92,109]. Tractography can be performed for the whole brain, or selectively using specific seeding and targeted regions of interest [109].

DTI tractography has been used to visualize the effect of MS lesions on the projection, association and commissural fibers [98]. MS patients exhibited an increase in ADC and reduction in FA, fiber density and streamline profiles within MS lesions and NAWM compared with healthy subjects, in which measures were correlated with the pattern of EDSS or clinical score of disability. Region-specific DTI tractography has also demonstrated sensitivity to functional changes: disruption of pyramidal and corticospinal tracts resulting in motor dysfunction [110]; disruption of left/right thalamic connectivity affecting working memory in early MS [111]. Tractography, however, has not been used to study animal models of MS.

Limitations of DWI studies in animal models

DWI studies of the mouse brain, either *ex vivo* [59,112] or *in vivo* [54,57,113] are based upon FA or orientation color-coded FA maps, rather than fiber tracking [114]. In addition, most of the fiber-tracking algorithms require high diffusion gradient weighting (b-values) and a large number of the applied diffusion-encoding gradients directions (high angular resolution diffusion imaging). This contributes significantly to the experiment time, and can be problematic for *in vivo* DWI involving unhealthy participants.

Ex vivo high angular resolution diffusion imaging may be a reasonable option when high-resolution, high number of directions and high b-values are required, but changes to tissue diffusion characteristics must be taken into consideration. In basic studies to compare *ex vivo* and *in vivo* rodent brain DWI, postfixation procedures have been shown to reduce the diffusivity measures in comparison to data obtained from *in vivo* imaging [115,116]. This difference may be due to variable tissue temperatures, microstructure properties, cell death and chemical fixation solution [117].

One recent study examined the difference between *in vivo* and *ex vivo* DTI in assessing the corpus callosum in both wild-type C57BL6 and cuprizone-induced mice. In control subjects, FA measurements were not significantly different between the *in vivo* and *ex vivo* samples; however, the diffusivity measurements (AD and RD) were drastically reduced in the *ex vivo* experiments [60]. Demyelination has been detected in the corpus callosum of cuprizone mice but there is little agreement between *in vivo* and *ex vivo* FA measurements. This study suggested that *ex vivo* RD serves as a potential indicator of demyelination better than *in vivo* RD, but *in vivo* AD is more reliable than *ex vivo* AD in detecting axonal injury [60].

The primary technical challenge of performing mouse brain DWI studies is achieving the required spatial resolution while preserving satisfactory S/N. This is especially important during the application of strong diffusion-encoding

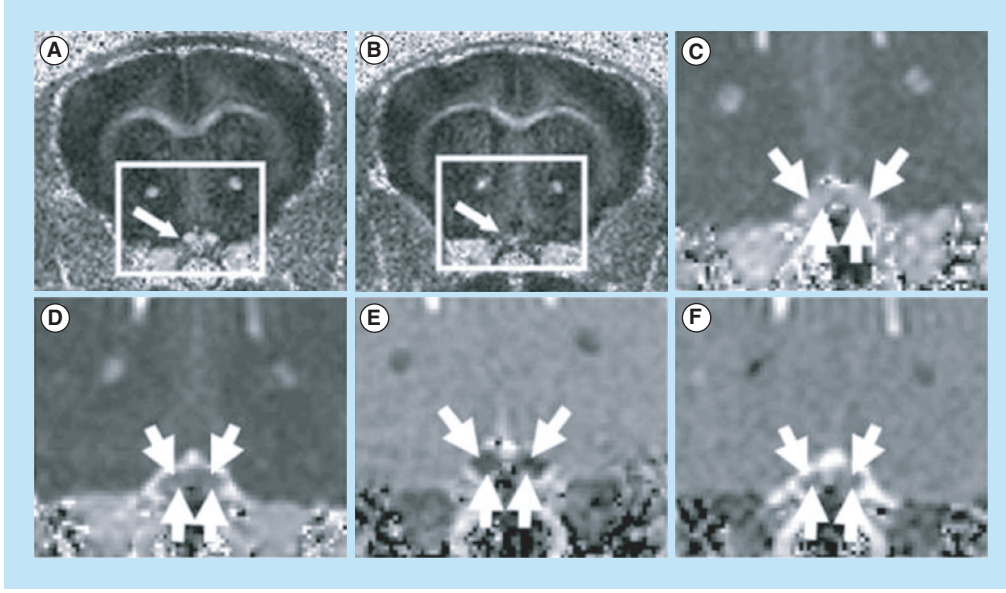

Figure 8. Assessment of optic nerve degeneration in experimental autoimmune encephalomyelitis mice using diffusion tensor imaging indices. A reduction in relative anisotropy value can be observed in the experimental autoimmune encephalomyelitis mouse **(B)** compared with the control subject **(A)**. Axial diffusivity decreases and radial diffusivity increases in the experimental autoimmune encephalomyelitis mouse; **(D)** and **(F)** respectively), in comparison with the control; **(C)** and **(E)**, respectively). Diffusion tensor imaging was acquired using Stejskal–Tanner sequence at 4.7 T, TR = 1.7 s, TE = 50 ms, six diffusion directions acquired with b-value = 838 s/mm^2, NEX = 4, slice thickness = 0.5 mm, FOV = 3 × 3 cm, and resolution = 59 × 59 × 500 μm^3 [57]. Boxed areas in **(A & B)** correspond to zoomed regions shown in **(C–F)**. The position of the optic nerves are shown by the arrows.
FOV: Field of view; NEX: Number of excitations; TE: Echo time; TR: Repetition time.

gradients, which results in significant signal attenuation and lower S/N. In addition, with high numbers of sampling diffusion-encoding directions, DWI requires a longer experiment time compared with other conventional MR imaging modalities [90]. In most cases, rodent DWI images are acquired at high magnetic field (>7 T) with small custom coils built to boost S/N. The use of higher magnetic fields brings undesired effects such as increased magnetic susceptibility and chemical shift artifacts, longer T_1 and shorter T_2 relaxation times [118]. DWI is inherently sensitive to motion to measure microscopic water displacement; and therefore, voluntary and involuntary movement can severely affect image quality. The use of respiratory gating and the navigator sequence has been developed to reduce these artifacts [119].

Assessing axonal pathology has become an integral and critical part in the diagnosis of MS. DW-MRI provides unique measurements of the distribution of water molecules in neural tissue, especially along the axons [120,121]. Recent advances of DWI-MRI involve development of axon density and diameter measurements in the WM of the living human brain, which potentially bring significant improvement to the detailed characterization of MR pathology [120,122]. However, challenges remain before DWI methods can be applied in clinical studies. These include the requirement for high-gradient amplitude (b > 3000 s/mm^2), relatively long imaging times to account for multiple diffusion directions and diffusion weightings and prior knowledge of the fiber orientation [122].

Compared to high resolutions T_1 or T_2 WI anatomical scans, DWI contains substantially higher partial volume effects. This makes comparison with histological sections, which has high in-plane resolutions (<5 μμ) and thin slices thickness (5–40 μμ), more difficult. Recent developments using 16.4 T ultra-high field imaging [112] and new gradient spin echo (GRASE) DWI sequences at 11.7 T can increase the resolutions of *ex vivo* DWI to 0.055 mm isotropic resolution [119]. A combination of GRASE and cryocoil at 11.7 T how pushed *in vivo* DWI to unprecedented 0.125 mm isotropic resolutions [123].

• Magnetization transfer imaging

MTI in MS patients

MTI is a quantitative MRI technique utilizing the interaction and exchange between mobile protons in a free water pool and protons in water bound to macromolecules, for example myelin structure. The magnetization transfer ratio (MTR) is measured by the incorporation of saturation pulses into the preparative part of a gradient echo or a spin echo sequence [51]. MTR analysis can be done through a whole brain voxel-based analysis (VBA) or using regions of interest, in which the MTR values are calculated from two sets of images acquired with and without the magnetization transfer saturation pulses [51]. MTI allows the depiction of several diffuse occult MS pathologies, for example, demyelination, gliosis and inflammation [124,125].

In MS patients [126] and animal models [17], pathology was detected as an abnormal reduction in MTR, which was suggested to reflect demyelination and axonal loss. However, MTR determination of MS-related pathology is somewhat nonspecific, because MTR reduction can also be caused by other pathological processes, such as edema, gliosis and inflammation [17,126].

Several groups [127,128] have investigated change in MTR and correlated it with lesion genesis and evolution. MTR reduction was observed a few months preceding observable Gd enhancement, and a further reduction in MTR for Gd-enhanced lesions has potential to highlight deteriorating MS lesions. MTR can be combined with conventional MRI methods, providing additional diagnostic value in predicting the evolution of T_1 WI hypointense lesions [127,128].

A modest reduction in MTR followed by a partial or complete recovery of MTR could indicate remyelination or other repair mechanisms during resolution of inflammation or gliosis [61]. Abnormal changes in MTR were also sensitive for detection of MS lesions within the normal-appearing WM and GM [61]. In another report [19], significant fluctuations in the MTR within active gadolinium-enhanced lesions were observed, consistent with the demyelination and remyelination process over a period of 3 years.

MTI in MS animal model

In a comparitive study of relapsing–remitting EAE using PLP and a chronic MOG-induced EAE, MTR histogram analysis of the whole brain showed a significant reduction in MTR values in early stage disease (13 days post immunization) [17]. Using VBA, MTR reduction was found in multiple brain regions such as the corpus callosum, caudate putamen and

hippocampus. These early remarkable changes may reflect widespread changes to the myelin structure [129]. However, as the disease progressed and during the chronic stages of the disease cycle (28 days post immunization), the reduction in MTR values was not significant, which could indicate less structural damage, initiation of the myelin repairing mechanism or interindividual variability between mice at the chronic stage [17].

On the other hand, in MOG chronic EAE, there was a reduction in MTR during three stages (11, 17 and 28 days post immunization) [17], emphasizing significant structural and axonal damage as a primary pathological process in the MOG-induced model and confirming similar changes observed in the spinal cord using the same EAE model [129,130]. The administration of glatiramer acetate (GA) to both the relapsing–remitting PLP and chronic MOG EAE groups showed that the MTR values recovered toward normal as in naïve animals **(Figure 9)**. These results support the role of MTR imaging as a marker of remyelination [17].

• Susceptibility weighted imaging

SWI in MS patients

Susceptibility differences between tissues offers a unique contrast [131]. SWI is based on T_2* WI, but comprises magnitude and phase information [132]. At sufficiently long echo time (TE), the signals from WM and GM, due to their different magnetic susceptibility, become out of phase. Therefore, phase imaging can be used to enrich the contrast between tissue types as well as accentuating iron-laden tissues and venous blood vessels [132,133].

A recent MS imaging study using T_2*-weighted imaging at 7 T [49] has explored the relationship between MS lesions and deep veins. The occurrence of plaque in association with deep veins has been established in previous histopathological studies, where the presence of the central vein or venule in the WM lesion was suggested to be a distinctive marker for differentiating between demyelinated MS lesions and non-MS lesions [49]. However, this technique requires investigation at lower field strength to assess its sensitivity in a clinically relevant environment. Susceptibility weighted angiography at 3 T [63] showed that central veins could be correlated with WM lesions with or without demyelination. Therefore, distinguishing the origin of central vein WM lesions from MS or other neuropathological changes is still problematic [63].

The role of perivenous space in developing MS lesions is still controversial [39,134–135]. Dynamic contrast-enhanced studies may provide a better understanding of the relationship between the central vein and MS lesions. Disruption of the BBB is an early-established MS lesion formation indicator [136]. However, it is not well defined whether the BBB disruption is the primary event that leads to lesion formation, or a secondary event that occurs after diffuse parenchymal tissue damage [39]. A recent study [136] has explored two patterns of enhanced lesions: new lesions tend to enhance centrifugally, whereas old lesions tend to enhance centripetally. This observation may be significant in resolving questions between opening and closing of the BBB; and also establishing whether vascular permeability could be used as a distinctive surrogate distinctive marker of acute and chronic lesions [135].

SWI in MS animal models

SWI hypointense lesions have been demonstrated in EAE mice immunized with $MOG_{35–55}$, CFA and PT [50]. These lesions were more prevalent in the lumbar spinal cord and cerebellum during the peak of disease severity at around days 16–19, as well as during long-term imaging at day 30 up to 6 months **(Figure 10)**. In addition, some of the lesions were no longer visible following perfusion; the percentages of the remaining lesions after perfusion were 60.1 and 46.6% in the spinal cord and cerebellum, respectively. This could be an indicator of the role of deoxyhemoglobin in the lumen vessels, in which they would have disappeared in *ex vivo* imaging [50]. Histopathology analyses of SWI hypointense lesions revealed iron deposition, inflammation and demyelination within the WM of the lumbar spinal cord, and inflammatory perivascular cuffs within the WM of the cerebellum [50].

Conclusion

This review paper highlights recent developments in MRI modalities tailored to investigate specific aspects of MS using animal models and to enhance diagnostic accuracy in patients. Key aspects of MS that can be monitored by MRI include BBB leakage, immune cell infiltration, inflammation, demyelination/remyelination, axonal injury, changes in brain connectivity and structural volumes [1,135].

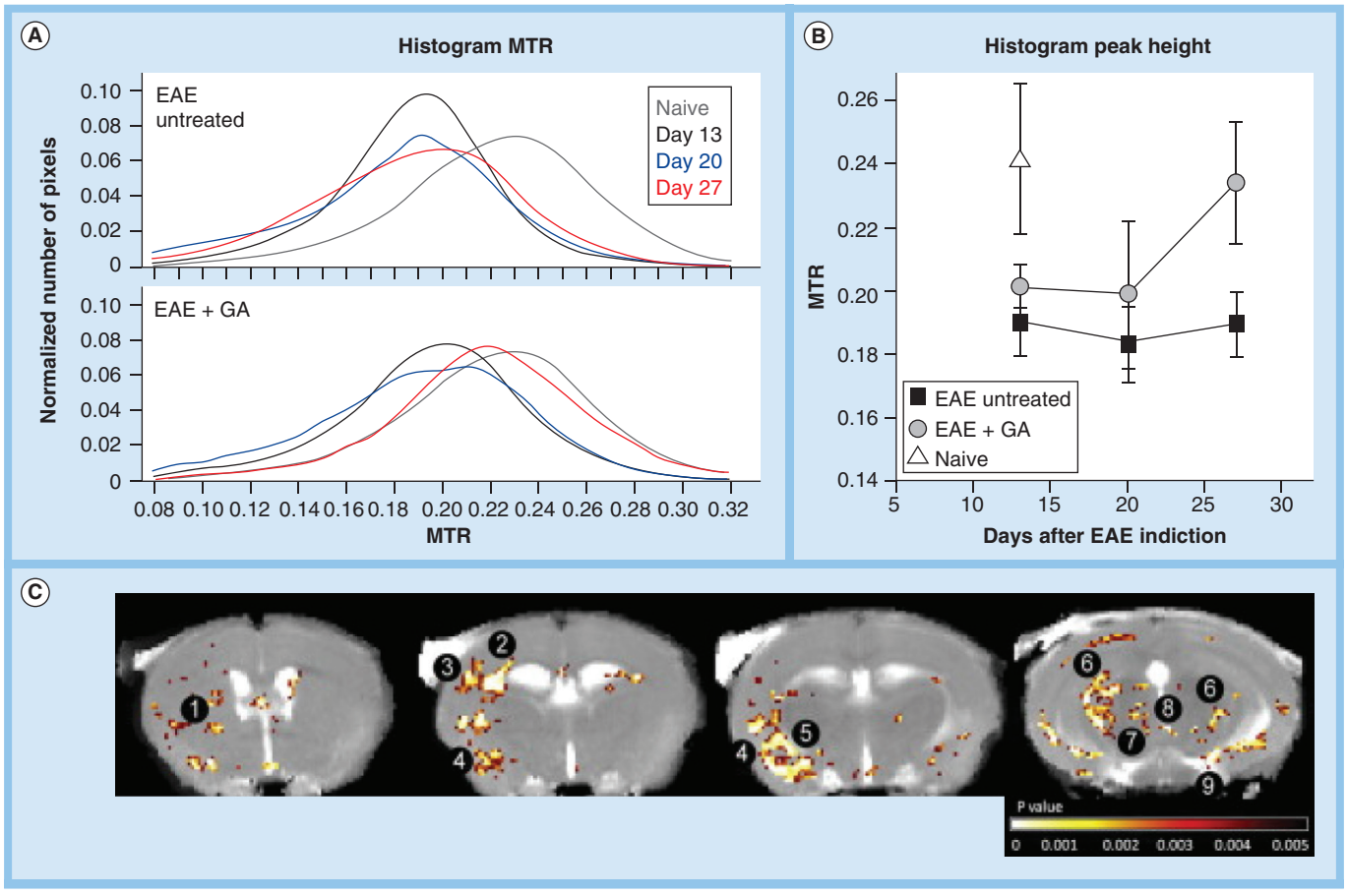

Figure 9. Magnetization transfer ratio is sensitive to detect the effect of glatirameracetate treatment in chronic MOG-induced experimental autoimmune encephalomyelitis. (A) Histogram of whole brain MTR showing changes of the MTR profile of EAE animals closer to naive animals after treatments with GA. **(B)** A corresponding graph showing changes of the MTR peak position from 0.19 to 0.24 (naive) after GA treatments. **(C)** Voxel-based analysis showing areas with significant MTR changes between GA treated and nontreated EAE animals [17]. Numbers 1–9 indicate caudate putamen, corpus callosum, sensory cortex, amygdala, piriform cortex, hippocampus, thalamus, deep mesencephalic nucleus and cerebral peduncle.
EAE: Experimental autoimmune encephalomyelitis; GA: Glatirameracetate; MTR: Magnetization transfer ratio.

In clinical settings, conventional MRI techniques are typically useful to detect established lesions in chronic MS, but they are generally insensitive during the initial stages of the disease [39]. Optimized methods such as FLAIR and DIR at high magnetic field strength provide improved sensitivity for detection of cortical lesions [11]. DWI can also detect such changes with additional advantages: sensitivity for detection of early MS especially in the normal-appearing WM or GM; and detection of changes in brain connectivity and fiber density with significant correlation with patient disability status [11,51]. MTR is sensitive to changes in myelin content, and can be useful in differentiating demyelinated from remyelinated lesions [19]. SWI provides unique contrasts by exploiting local susceptibility changes due to MS lesions and may become an increasingly important technique, particularly at higher field strength [14]. Recent detection of central veins near NAWM using SWI remains controversial [63].

Longitudinal MRI imaging of rodent models of MS facilitate investigation of temporal changes in the brain during progression from the acute to the chronic stages of MS disease. In general, MRI findings observed in patients with MS patients have been similarly observed in rodent models of MS. These include T_2 hypointensity of the deep GM lesions [41], USPIO detection of immune cell infiltration [48], reduction in FA due to demyelination [57], brain atrophy [46], partial increasing of MTR as indicator of tissue repairing [126] and characterization of iron deposition using SWI [137].

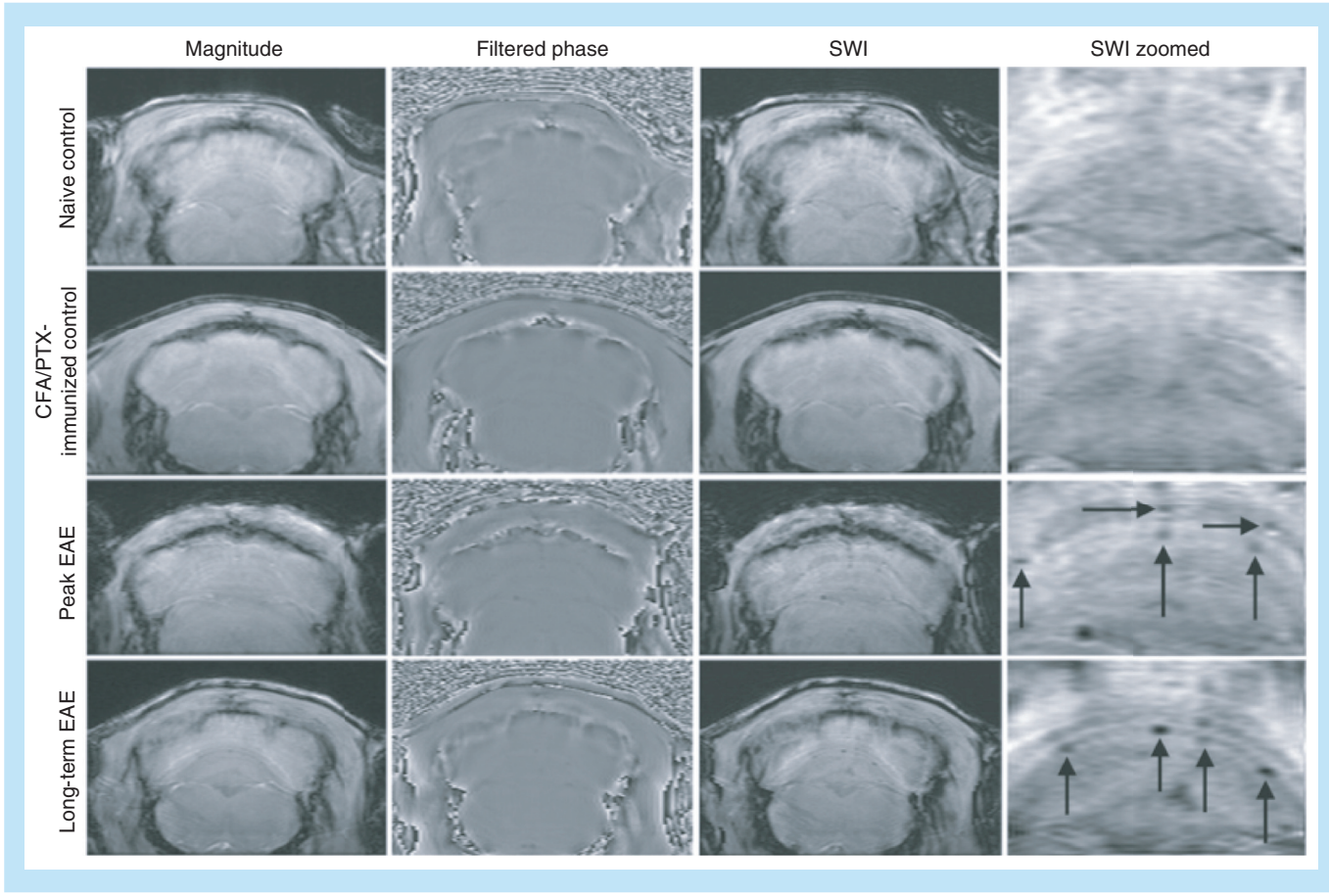

Figure 10. Visualization of susceptibility-weighted imaging hypointense lesions in the cerebellar white matter of experimental autoimmune encephalomyelitis mice, multiple sclerosis lesions can be observed in susceptibility-weighted imaging (zoomed column) during the peak experimental autoimmune encephalomyelitis (18 days postimmunization) and long-term disease progression (6 months postimmunization). These lesions (black arrows) have not been detected in the naive and control mice immunized with complete Freud adjuvant and pertussis toxin. SWI was acquired using 3D gradient echo flow compensated at 9.4 T, imaging parameters: TR/TE = 50/4 ms, fractional anisotropy = 15°, NEX = 17, FOV = 0.92 × 1.28 × 1.28, voxel size = 48 × 100 × 400 μm^3) [50].
CFA: Complete Freud's adjuvant; EAE: Experimental autoimmune encephalomyelitis; FOV: Field of view; GA: Glatirameracetate; MS: Multiple sclerosis; MTR: Magnetization transfer ratio; NEX: Number of excitations; PTX: Pertussis toxin; SWI: susceptibility weighted imaging; TE: Echo time; TR: Repetition time.

Future perspective

Clinical diagnosis and preclinical research in MS will continue to benefit from further development and optimization of MRI technology at high-field strengths. The increased signal to noise and improved RF coil technology, including the emergence of transmit/receive phased arrays, is providing better sensitivity and imaging at higher spatial resolution with reduced partial volume effects allowing improved detection and characterization of small lesions in normal-appearing WM/GM. For human MRI, 3-T scanners are becoming more widely available in clinics, while 7-T scanners are increasingly used in research and >9.4-T dedicated human brain MRI scanners for cutting-edge research have appeared [14]. For preclinical and basic research, 9.4-T mouse brain cryogenic coils for *in vivo* imaging and ultra-high field >11.7-T scanners for *ex vivo* imaging will improve characterization of novel animal models of MS. New-generation MRI scanners are equipped with multichannel transmit/receive coils for faster acquisition and stronger gradients to allow diffusion imaging with higher b-values and demanding applications such as oscillating diffusion gradient imaging [138]. New analysis methods in diffusion MRI including diffusion kurtosis [139], neurite orientation dispersion and density imaging (NODDI) [140] and axon diameter and density

measurements [122], informed by new data from the human CONNECTOME project [141] and high-resolution mouse brain and spinal cord atlases [76] will allow enhanced characterization of changes in nervous tissue components and observation of cell infiltration into nervous tissues.

Recent development of multimodal MRI/PET scanners for human and animal imaging [142,143] allows simultaneous MRI and PET signal detection of MRI markers and radioligands. This emerging technology holds great potential in the examination of specific aspects of inflammation, axonal degeneration or repair and changes in neurometabolism for enhanced characterization of MS and testing of potential intervention therapies. Translation of these new imaging modalities to the clinic remains a goal for the next decade.

Financial & competing interests disclosure

The authors have no relevant affiliations or financial involvement with any organization or entity with a financial interest in or financial conflict with the subject matter or materials discussed in the manuscript. This includes employment, consultancies, honoraria, stock ownership or options, expert testimony, grants or patents received or pending or royalties.

No writing assistance was utilized in the production of this manuscript.

EXECUTIVE SUMMARY

MRI studies of rodent models of multiple sclerosis present specific opportunities, challenges & advantages

- Rodent models allow detailed longitudinal studies to examine specific aspect of multiple sclerosis (MS), where histopathological analyses can be performed to corroborate the source of the MRI signal change in the tissue.
- Similar to human MRI, a combination of MS pathological events in mice such as demyelination, remyelination, axonal loss, immune cell activity, extravasated blood and tissue edema can affect both T_1 and T_2 contrast and can confound their interpretation.
- To visualize brain microstructures in mice within the limitations of general anesthesia and respiratory motion, 2D high in-plane resolution images are often acquired but with considerable partial volume effects.
- 3D *ex vivo* images of the brain and spinal cord from perfused mouse models of MS can provide isotropic high-resolution images. However, tissue fixation methods can affect diffusion parameters and should be carefully considered.
- The use of ultra high-field magnets improves S/N but at the expense of increased susceptibility and chemical shift artifacts. Using a cryogenic probe for mouse brain imaging at 9.4 T dramatically improves S/N to allow more detailed characterization of CNS lesions in mouse models of MS.

MRI has played major roles in characterizing pathological changes in rodent models of MS & MRI signal changes are associated with specific or several pathological events

- T_1 signal intensities were negatively correlated with the cell densities of microglia and astrocytes. Lesions with strong T_1 hypointensity (blackholes) represent areas with severe tissue damage with axonal and neuronal loss.
- T_2 signal intensities were positively correlated with the density of activated microglia cells, reactive astrocytes and immunoglobin deposition. T_2 hypointensity lesions in deep brain GM could be associated with extravasated blood and have some correlations with clinical disabilities.
- Gd contrast agent is useful for detecting increased permeability of the blood–brain barrier, whereas iron paramagnetic nanoparticles are useful to detect macrophage infiltration into damaged tissues.
- Diffusion-weighted imaging is sensitive for detection of lesions in normal-appearing white matter and normal-appearing gray matter. Decreasing axial diffusivity and increasing radial diffusivity are established respective indicators of axonal damage and demyelination. Fractional anisotropy generally decreases with demyelination, although a significant increase of fractional anisotropy has been reported in cortical lesions.
- Magnetization transfer ratio is sensitive for measuring myelin content to detect demyelination and remyelination in experimental autoimmune encephalomyelitis mouse models.
- Susceptibility-weighted imaging exploited susceptibility variations from local tissue iron content of myelin and blood, and to detect demyelination and increased vascular size near lesions.

References

1 Lassmann H. Pathology and disease mechanisms in different stages of multiple sclerosis. *J. Neurol. Sci.* 333(1–2), 1–4 (2013).

2 Khan N, Smith MT. Multiple sclerosis-induced neuropathic pain: pharmacological management and pathophysiological insights from rodent EAE models. *Inflammopharmacology* 22(1), 1–22 (2013).

3 Trapp BD, Nave KA. Multiple sclerosis: an immune or neurodegenerative disorder? *Annu. Rev. Neurosci.* 31, 247–269 (2008).

4 MS Research Australia. Living with MS. www.msra.org.au/living-ms

5 Campbell JD, Ghushchyan V, Brett Mcqueen R *et al.* Burden of multiple sclerosis on direct, indirect costs and quality of life: national US estimates. *Mult. Scler. Relat. Disord.* 3(2), 227–236 (2014).

6 Hauser SL, Chan JR, Oksenberg JR. Multiple sclerosis: prospects and promise. *Ann. Neurol.* 74(3), 317–327 (2013).

7 Shivane AG, Chakrabarty A. Multiple sclerosis and demyelination. *Curr. Diagn. Pathol.* 13(3), 193–202 (2007).

8 Chao M, Ramagopalan S, Herrera B *et al.* MHC transmission: insights into gender bias in MS susceptibility. *Neurology* 76(3), 242–246 (2011).

9 Filippi M, Rocca MA, Barkhof F *et al.* Association between pathological and MRI findings in multiple sclerosis. *Lancet Neurol.* 11(4), 349–360 (2012).

10 Seewann A, Kooi E-J, Roosendaal S *et al.* Postmortem verification of MS cortical lesion detection with 3D DIR. *Neurology* 78(5), 302–308 (2012).

11 Calabrese M, Rinaldi F, Seppi D *et al.* Cortical diffusion-tensor imaging abnormalities in multiple sclerosis: a 3-year longitudinal study. *Radiology* 261(3), 891–898 (2011).

12 Geurts JJG, Pouwels PJW, Uitdehaag BMJ, Polman CH, Barkhof F, Castelijns JA. Intracortical lesions in multiple sclerosis: improved detection with 3D double inversion-recovery MR imaging1. *Radiology* 236(1), 254–260 (2005).

13 Kilsdonk I, De Graaf W, Soriano AL *et al.* Multicontrast MR imaging at 7T in multiple sclerosis: highest lesion detection in cortical gray matter with 3D-FLAIR. *Am. J. Neuroradiol.* 34(4) 791–796 (2012).

14 Filippi M, Evangelou N, Kangarlu A *et al.* Ultra-high-field MR imaging in multiple sclerosis. *J. Neurol. Neurosurg. Psychiatry* 85(1), 60–66 (2014).

15 Sethi V, Yousry TA, Muhlert N *et al.* Improved detection of cortical MS lesions with phase-sensitive inversion recovery MRI. *J. Neurol. Neurosurg. Psychiatry* 83(9), 877–882 (2012).

16 Sinnecker T, Bozin I, Dörr J *et al.* Periventricular venous density in multiple sclerosis is inversely associated with T2 lesion count: a 7 Tesla MRI study. *Mult. Scler.* 19(3), 316–325 (2013).

17 Aharoni R, Sasson E, Blumenfeld-Katzir T *et al.* Magnetic resonance imaging characterization of different experimental autoimmune encephalomyelitis models and the therapeutic effect of glatiramer acetate. *Exp. Neurol.* 240(0), 130–144 (2013).

18 Dousset V, Brochet B, Deloire M *et al.* MR imaging of relapsing multiple sclerosis patients using ultra-small-particle iron oxide and compared with gadolinium. *Am. J. Neuroradiol.* 27(5), 1000–1005 (2006).

19 Chen JT, Collins DL, Atkins HL, Freedman MS, Arnold DL. Magnetization transfer ratio evolution with demyelination and remyelination in multiple sclerosis lesions. *Ann. Neurol.* 63(2), 254–262 (2008).

20 Hammond KE, Metcalf M, Carvajal L *et al.* Quantitative *in vivo* magnetic resonance imaging of multiple sclerosis at 7 Tesla with sensitivity to iron. *Ann. Neurol.* 64(6), 707–713 (2008).

21 Pantano P. DTI measurements in multiple sclerosis: evaluation of brain damage and clinical implications. *Mult. Scler. Int.* 2013, 671730 (2013).

22 Ge Y, Law M, Grossman RI. Applications of diffusion tensor MR imaging in multiple sclerosis. *Ann. NY Acad. Sci.* 1064(1), 202–219 (2006).

23 Altmann DM, Boyton RJ. Models of multiple sclerosis. *Drug Discov. Today* 1(4), 405–410 (2004).

24 Mix E, Meyer-Rienecker H, Hartung HP, Zettl UK. Animal models of multiple sclerosis – potentials and limitations. *Prog. Neurobiol.* 92(3), 386–404 (2010).

25 Denic A, Johnson AJ, Bieber AJ, Warrington AE, Rodriguez M, Pirko I. The relevance of animal models in multiple sclerosis research. *Pathophysiology* 18(1), 21–29 (2011).

26 Nelson A, Bieber A, Rodriguez M. Contrasting murine models of MS. *Int. MS J.* 11(3), 95–99 (2004).

27 Kipp M, Clarner T, Dang J, Copray S, Beyer C. The cuprizone animal model: new insights into an old story. *Acta Neuropathol.* 118(6), 723–736 (2009).

28 Bieber AJ, Kerr S, Rodriguez M. Efficient central nervous system remyelination requires T cells. *Ann. Neurol.* 53(5), 680–684 (2003).

29 Rivers TM, Sprunt D, Berry G. Observations on attempts to produce acute disseminated encephalomyelitis in monkeys. *J. Exp. Med.* 58(1), 39–53 (1933).

30 Pettinelli C, McFarlin D. Adoptive transfer of experimental allergic encephalomyelitis in SJL/J mice after *in vitro* activation of lymph node cells by myelin basic protein: requirement for Lyt 1+ 2-T lymphocytes. *J. Immunol.* 127(4), 1420–1423 (1981).

31 Kipp M, Van Der Star B, Vogel D *et al.* Experimental *in vivo* and *in vitro* models of multiple sclerosis: EAE and beyond. *Mult. Scler. Relat. Disord.* 1(1), 15–28 (2012).

32 Hauser SL, Bhan AK, Gilles F, Kemp M, Kerr C, Weiner HL. Immunohistochemical analysis of the cellular infiltrate in multiple sclerosis lesions. *Ann. Neurol.* 19(6), 578–587 (1986).

33 Neumann H, Medana IM, Bauer J, Lassmann H. Cytotoxic T lymphocytes in autoimmune and degenerative CNS diseases. *Trends Neurosci.* 25(6), 313–319 (2002).

34 Rodriguez M, Oleszak E, Leibowitz J. Theiler's murine encephalomyelitis: a model of demyelination and persistence of virus. *Crit. Rev. Immunol.* 7(4), 325 (1987).

35 Ure DR, Rodriguez M. Polyreactive antibodies to glatiramer acetate promote myelin repair in murine model of demyelinating disease. *FASEB J.* 16(10), 1260–1262 (2002).

36 Mackenzie-Graham A. *In vivo* vs. *ex vivo* magnetic resonance imaging in mice. *Front. Neuroinform.* 6, 19 (2012).

37 Pirko I, Nolan TK, Holland SK, Johnson AJ. Multiple sclerosis: pathogenesis and MR imaging features of T1 hypointensities in murine model1. *Radiology* 246(3), 790–795 (2008).

38 Von Elverfeldt D, Reichardt W, Harsan L. Molecular and translational research. In: *High-Field MR Imaging.* Springer, Heidelberg, Germany, 229–258 (2012).

39 Ceccarelli A, Bakshi R, Neema M. MRI in multiple sclerosis: a review of the current literature. *Curr. Opin. Neurol.* 25(4), 402–409 (2012).

40 Bakshi R, Dmochowski J, Shaikh ZA, Jacobs L. Gray matter T2 hypointensity is related to plaques and atrophy in the brains of multiple sclerosis patients. *J. Neurol. Sci.* 185(1), 19–26 (2001).

41 Pirko I, Johnson AJ, Lohrey AK, Chen Y, Ying J. Deep gray matter T2 hypointensity

correlates with disability in a murine model of MS. *J. Neurol. Sci.* 282(1–2), 34–38 (2009).

42 Ge Y, Grossman RI, Udupa JK *et al.* Brain atrophy in relapsing–remitting multiple sclerosis and secondary progressive multiple sclerosis: longitudinal quantitative analysis. *Radiology* 214(3), 665–670 (2000).

43 Rudick R, Fisher E, Lee JC, Simon J, Jacobs L. Use of the brain parenchymal fraction to measure whole brain atrophy in relapsing–remitting MS. *Neurology* 53(8), 1698–1698 (1999).

44 Stevenson V, Miller D, Leary S *et al.* One year follow up study of primary and transitional progressive multiple sclerosis. *J. Neurol. Neurosurg. Psychiatry* 68(6), 713–718 (2000).

45 Mackenzie-Graham A, Tiwari-Woodruff SK, Sharma G *et al.* Purkinje cell loss in experimental autoimmune encephalomyelitis. *NeuroImage* 48(4), 637–651 (2009).

46 Mackenzie-Graham A, Rinek GA, Avedisian A *et al.* Cortical atrophy in experimental autoimmune encephalomyelitis: *in vivo* imaging. *NeuroImage* 60(1), 95–104 (2012).

47 Vellinga MM, Engberink RDO, Seewann A *et al.* Pluriformity of inflammation in multiple sclerosis shown by ultra-small iron oxide particle enhancement. *Brain* 131(3), 800–807 (2008).

48 Brochet B, Deloire M, Touil T *et al.* Early macrophage MRI of inflammatory lesions predicts lesion severity and disease development in relapsing EAE. *NeuroImage* 32(1), 266–274 (2006).

49 Tallantyre E, Dixon J, Donaldson I *et al.* Ultra-high-field imaging distinguishes MS lesions from asymptomatic white matter lesions. *Neurology* 76(6), 534–539 (2011).

50 Nathoo N, Agrawal S, Wu Y *et al.* Susceptibility-weighted imaging in the experimental autoimmune encephalomyelitis model of multiple sclerosis indicates elevated deoxyhemoglobin, iron deposition and demyelination. *Mult. Scler.* 19(6), 721–731 (2012).

51 Bakshi R, Minagar A, Jaisani Z, Wolinsky JS. Imaging of multiple sclerosis: role in neurotherapeutics. *NeuroRx* 2(2), 277–303 (2005).

52 Nessler S, Boretius S, Stadelmann C *et al.* Early MRI changes in a mouse model of multiple sclerosis are predictive of severe inflammatory tissue damage. *Brain* 130(8), 2186 (2007).

53 Rovaris M, Gass A, Bammer R *et al.* Diffusion MRI in multiple sclerosis. *Neurology* 65(10), 1526 (2005).

54 Wu QZ, Yang Q, Cate HS *et al.* MRI identification of the rostral-caudal pattern of pathology within the corpus callosum in the cuprizone mouse model. *J. Magn. Reson. Imaging* 27(3), 446–453 (2007).

55 Hygino CLC Jr, Batista RR, Domingues RC, Barkhof F. Diffusion magnetic resonance imaging in multiple sclerosis. *Neuroimaging Clin. N. Am.* 21(1), 71 (2011).

56 Pagani E, Bammer R, Horsfield MA *et al.* Diffusion MR imaging in multiple sclerosis: technical aspects and challenges. *Am. J. Neuroradiol.* 28(3), 411 (2007).

57 Sun SW, Liang HF, Schmidt RE, Cross AH, Song SK. Selective vulnerability of cerebral white matter in a murine model of multiple sclerosis detected using diffusion tensor imaging. *Neurobiol. Dis.* 28(1), 30–38 (2007).

58 Roosendaal S, Geurts J, Vrenken H *et al.* Regional DTI differences in multiple sclerosis patients. *NeuroImage* 44(4), 1397–1403 (2009).

59 Song SK, Yoshino J, Le TQ *et al.* Demyelination increases radial diffusivity in corpus callosum of mouse brain. *NeuroImage* 26(1), 132–140 (2005).

60 Zhang J, Jones MV, Mcmahon MT, Mori S, Calabresi PA. *In vivo* and *ex vivo* diffusion tensor imaging of cuprizone-induced demyelination in the mouse corpus callosum. *Magn. Reson. Med.* 67(3), 750–759 (2012).

61 Miller D, Thompson A, Filippi M. Magnetic resonance studies of abnormalities in the normal appearing white matter and grey matter in multiple sclerosis. *J. Neurol.* 250(12), 1407–1419 (2003).

62 Horsfield MA, Barker GJ, Barkhof F, Miller DH, Thompson AJ, Filippi M. Guidelines for using quantitative magnetization transfer magnetic resonance imaging for monitoring treatment of multiple sclerosis. *J. Magn. Reson. Imaging* 17(4), 389–397 (2003).

63 Lummel N, Boeckh-Behrens T, Schoepf V, Burke M, Brückmann H, Linn J. Presence of a central vein within white matter lesions on susceptibility weighted imaging: a specific finding for multiple sclerosis? *Neuroradiology* 53(5), 311–317 (2011).

64 Pirko I, Johnson AJ, Chen Y *et al.* Brain atrophy correlates with functional outcome in a murine model of multiple sclerosis. *NeuroImage* 54(2), 802–806 (2011).

65 Xie M, Tobin JE, Budde MD *et al.* Rostrocaudal analysis of corpus callosum demyelination and axon damage across disease stages refines diffusion tensor imaging correlations with pathological features. *J. Neuropathol. Exp. Neurol.* 69(7), 704–716 (2010).

66 Johnson HL, Chen Y, Jin F *et al.* CD8 T cell-initiated blood–brain barrier disruption is independent of neutrophil support. *J. Immunol.* 189(4), 1937–1945 (2012).

67 Fisniku L, Brex P, Altmann D *et al.* Disability and T2 MRI lesions: a 20-year follow-up of patients with relapse onset of multiple sclerosis. *Brain* 131(3), 808–817 (2008).

68 Sriram S, Steiner I. Experimental allergic encephalomyelitis: a misleading model of multiple sclerosis. *Ann. Neurol.* 58(6), 939–945 (2005).

69 Neema M, Stankiewicz J, Arora A *et al.* T1-and T2-based MRI measures of diffuse gray matter and white matter damage in patients with multiple sclerosis. *J. Neuroimaging* 17, 16S–21S (2007).

70 Zhang Y, Zabad R, Wei X, Metz L, Hill M, Mitchell J. Deep grey matter black T2 on 3 tesla magnetic resonance imaging correlates with disability in multiple sclerosis. *Mult. Scler.* 13(7), 880–883 (2007).

71 Brass S, Benedict RHB, Weinstock-Guttman B, Munschauer F, Bakshi R. Cognitive impairment is associated with subcortical magnetic resonance imaging grey matter T2 hypointensity in multiple sclerosis. *Mult. Scler.* 12(4), 437–444 (2006).

72 De Groot C, Bergers E, Kamphorst W *et al.* Post-mortem MRI-guided sampling of multiple sclerosis brain lesions increased yield of active demyelinating and (p) reactive lesions. *Brain* 124(8), 1635–1645 (2001).

73 Traboulsee A, Li DK, Zhao G, Paty DW. Conventional MRI techniques in multiple sclerosis. In: *MR Imaging in White Matter Diseases of the Brain and Spinal Cord*. Springer, NY, USA, 211–223 (2005).

74 Kutzelnigg A, Faber-Rod JC, Bauer J *et al.* Widespread demyelination in the cerebellar cortex in multiple sclerosis. *Brain Pathol.* 17(1), 38–44 (2007).

75 Mackenzie-Graham A, Tinsley MR, Shah KP *et al.* Cerebellar cortical atrophy in experimental autoimmune encephalomyelitis. *NeuroImage* 32(3), 1016–1023 (2006).

76 Ullmann JF, Watson C, Janke AL, Kurniawan ND, Reutens DC. A segmentation protocol and MRI atlas of the C57BL/6J mouse neocortex. *NeuroImage* 78, 196–203 (2013).

77 Sati P, George IC, Shea CD, Gaitán MI, Reich DS. FLAIR*: a combined MR contrast technique for visualizing white matter lesions and parenchymal veins. *Radiology* 265(3), 926–932 (2012).

78 De Graaf WL, Kilsdonk ID, Lopez-Soriano A *et al.* Clinical application of multi-contrast 7-T MR imaging in multiple sclerosis: increased lesion detection compared with 3 T confined to grey matter. *Eur. Radiol.* 23(2), 528–540 (2013).

79 Waiczies H, Millward JM, Lepore S *et al.* Identification of cellular infiltrates during early stages of brain inflammation with magnetic resonance microscopy. *PLoS ONE* 7(3), e32796 (2012).

80 Bjartmar C, Kinkel RP, Kidd G, Rudick RA, Trapp BD. Axonal loss in normal-appearing white matter in a patient with acute MS. *Neurology* 57(7), 1248–1252 (2001).

81 Aggarwal M, Zhang J, Mori S. Chapter 15: magnetic resonance imaging of the mouse brain. In: *The Mouse Nervous System.* Charles W, George P, Luis P (Eds). Academic Press, CA, USA, 473–488 (2012).

82 Nouls JC, Izenson MG, Greeley HP, Johnson GA. Design of a superconducting volume coil for magnetic resonance microscopy of the mouse brain. *J. Magn. Reson.* 191(2), 231–238 (2008).

83 Baltes C, Radzwill N, Bosshard S, Marek D, Rudin M. Micro MRI of the mouse brain using a novel 400 MHz cryogenic quadrature RF probe. *NMR Biomed.* 22(8), 834–842 (2009).

84 Corot C, Robert P, Idee JM, Port M. Recent advances in iron oxide nanocrystal technology for medical imaging. *Adv. Drug Deliv. Rev.* 58(14), 1471–1504 (2006).

85 Metz S, Bonaterra G, Rudelius M, Settles M, Rummeny EJ, Daldrup-Link HE. Capacity of human monocytes to phagocytose approved iron oxide MR contrast agents *in vitro*. *Eur. Radiol.* 14(10), 1851–1858 (2004).

86 Johnson HL, Jin F, Pirko I, Johnson AJ. Theiler's murine encephalomyelitis virus as an experimental model system to study the mechanism of blood–brain barrier disruption. *J. Neurovirol.* 20(2), 107–112 (2013).

87 Winston GP. The physical and biological basis of quantitative parameters derived from diffusion MRI. *Quant. Imaging Med. Surg.* 2(4), 254 (2012).

88 Mori S, Tournier J. Chapter 4: principle of diffusion tensor imaging. In: *Introduction to Diffusion Tensor Imaging (2nd Edition).* Academic Press, CA, USA, 27–32 (2014).

89 Mori S, Zhang J. Principles of diffusion tensor imaging and its applications to basic neuroscience research. *Neuron* 51(5), 527–539 (2006).

90 Zhang J, Aggarwal M, Mori S. Structural insights into the rodent CNS via diffusion tensor imaging. *Trends Neurosci.* 35(7), 412–421 (2012).

91 Aung WY, Mar S, Benzinger TL. Diffusion tensor MRI as a biomarker in axonal and myelin damage. *Imaging in Med.* 5(5), 427–440 (2013).

92 Tournier JD, Mori S, Leemans A. Diffusion tensor imaging and beyond. *Magn. Reson. Med.* 65(6), 1532–1556 (2011).

93 Bammer R, Augustin M, Strasser-Fuchs S *et al.* Magnetic resonance diffusion tensor imaging for characterizing diffuse and focal white matter abnormalities in multiple sclerosis. *Magn. Reson. Med.* 44(4), 583–591 (2000).

94 Castriota-Scanderbeg A, Sabatini U, Fasano F *et al.* Diffusion of water in large demyelinating lesions: a follow-up study. *Neuroradiology* 44(9), 764–767 (2002).

95 Kolind SH, Laule C, Vavasour IM *et al.* Complementary information from multi-exponential T2 relaxation and diffusion tensor imaging reveals differences between multiple sclerosis lesions. *NeuroImage* 40(1), 77–85 (2008).

96 Trapp BD, Peterson J, Ransohoff RM, Rudick R, Mörk S, Bö L. Axonal transection in the lesions of multiple sclerosis. *N. Engl. J. Med.* 338(5), 278–285 (1998).

97 Bergers E, Bot J, De Groot C *et al.* Axonal damage in the spinal cord of MS patients occurs largely independent of T2 MRI lesions. *Neurology* 59(11), 1766–1771 (2002).

98 Hu B, Ye B, Yang Y *et al.* Quantitative diffusion tensor deterministic and probabilistic fiber tractography in relapsing–remitting multiple sclerosis. *Eur. J. Radiol.* 79(1), 101–107 (2011).

99 Koenig KA, Sakaie KE, Lowe MJ *et al.* High spatial and angular resolution diffusion-weighted imaging reveals forniceal damage related to memory impairment. *Magn. Reson. Imaging* 31(5), 695–699 (2013).

100 Inglese M, Bester M. Diffusion imaging in multiple sclerosis: research and clinical implications. *NMR Biomed.* 23(7), 865–872 (2010).

101 Song SK, Sun SW, Ramsbottom MJ, Chang C, Russell J, Cross AH. Dysmyelination revealed through MRI as increased radial (but unchanged axial) diffusion of water. *NeuroImage* 17(3), 1429–1436 (2002).

102 Song SK, Sun SW, Ju WK, Lin SJ, Cross AH, Neufeld AH. Diffusion tensor imaging detects and differentiates axon and myelin degeneration in mouse optic nerve after retinal ischemia. *NeuroImage* 20(3), 1714–1722 (2003).

103 Kim JH, Budde MD, Liang HF *et al.* Detecting axon damage in spinal cord from a mouse model of multiple sclerosis. *Neurobiol. Dis.* 21(3), 626–632 (2006).

104 Sun SW, Liang HF, Cross AH, Song SK. Evolving Wallerian degeneration after transient retinal ischemia in mice characterized by diffusion tensor imaging. *NeuroImage* 40(1), 1–10 (2008).

105 Xu J, Sun SW, Naismith RT, Snyder AZ, Cross AH, Song SK. Assessing optic nerve pathology with diffusion MRI: from mouse to human. *NMR Biomed.* 21(9), 928–940 (2008).

106 Wang Y, Wang Q, Haldar JP *et al.* Quantification of increased cellularity during inflammatory demyelination. *Brain* 134(12), 3590–3601 (2011).

107 Harsan LA, Paul D, Schnell S *et al. In vivo* diffusion tensor magnetic resonance imaging and fiber tracking of the mouse brain. *NMR Biomed.* 23(7), 884–896 (2010).

108 Johansen-Berg H, Rushworth MF. Using diffusion imaging to study human connectional anatomy. *Ann. Rev. Neurosci.* 32, 75–94 (2009).

109 Tournier J, Calamante F, Connelly A. MRtrix: Diffusion tractography in crossing fiber regions. *Int. J. Imaging Syst. Technol.* 22(1), 53–66 (2012).

110 Lin F, Yu C, Jiang T, Li K, Chan P. Diffusion tensor tractography-based group mapping of the pyramidal tract in relapsing–remitting multiple sclerosis patients. *Am. J. Neuroradiol.* 28(2), 278–282 (2007).

111 Audoin B, Guye M, Reuter F *et al.* Structure of WM bundles constituting the working memory system in early multiple sclerosis: a quantitative DTI tractography study. *NeuroImage* 36(4), 1324–1330 (2007).

112 Moldrich RX, Pannek K, Hoch R, Rubenstein JL, Kurniawan ND, Richards LJ. Comparative mouse brain tractography of diffusion magnetic resonance imaging. *NeuroImage* 51(3), 1027–1036 (2010).

113 Boretius S, Escher A, Dallenga T *et al.* Assessment of lesion pathology in a new animal model of MS by multiparametric MRI and DTI. *NeuroImage* 59(3), 2678–2688 (2012).

114 Zhang J. Diffusion tensor imaging of white matter pathology in the mouse brain. *Imaging* 2(6), 623–632 (2010).

115 Sun SW, Neil JJ, Song SK. Relative indices of water diffusion anisotropy are equivalent in live and formalin-fixed mouse brains. *Magn. Reson. Med.* 50(4), 743–748 (2003).

116 Sun SW, Neil JJ, Liang HF *et al.* Formalin fixation alters water diffusion coefficient

magnitude but not anisotropy in infarcted brain. *Magn. Reson. Med.* 53(6), 1447–1451 (2005).

117 Shepherd TM, Thelwall PE, Stanisz GJ, Blackband SJ. Aldehyde fixative solutions alter the water relaxation and diffusion properties of nervous tissue. *Magn. Reson. Med.* 62(1), 26–34 (2009).

118 Pirko I, Fricke ST, Johnson AJ, Rodriguez M, Macura SI. Magnetic resonance imaging microscopy, and spectroscopy of the central nervous system in experimental animals. *NeuroRx* 2(2), 250–264 (2005).

119 Aggarwal M, Mori S, Shimogori T, Blackshaw S, Zhang J. Three dimensional diffusion tensor microimaging for anatomical characterization of the mouse brain. *Magn. Reson. Med.* 64(1), 249–261 (2010).

120 Caminiti R, Carducci F, Piervincenzi C *et al.* Diameter, length, speed, and conduction delay of callosal axons in macaque monkeys and humans: comparing data from histology and magnetic resonance imaging diffusion tractography. *J. Neurosci.* 33(36), 14501–14511 (2013).

121 Barazany D, Basser PJ, Assaf Y. *In vivo* measurement of axon diameter distribution in the corpus callosum of rat brain. *Brain* 132(5), 1210–1220 (2009).

122 Alexander DC, Hubbard PL, Hall MG *et al.* Orientationally invariant indices of axon diameter and density from diffusion MRI. *NeuroImage* 52(4), 1374–1389 (2010).

123 Wu D, Xu J, McMahon MT *et al. In vivo* high-resolution diffusion tensor imaging of the mouse brain. *NeuroImage* 83(0), 18–26 (2013).

124 Abdel-Fahim R, Mistry N, Mougin O *et al.* Improved detection of focal cortical lesions using 7T magnetisation transfer imaging in patients with multiple sclerosis. *Mult. Scler. Relat. Disord.* doi:10.1016/j.msard.2013.10.004 (2013) (Epub ahead of print).

125 Bakshi R, Thompson AJ, Rocca MA *et al.* MRI in multiple sclerosis: current status and future prospects. *Lancet Neurol.* 7(7), 615–625 (2008).

126 Button T, Altmann D, Tozer D *et al.* Magnetization transfer imaging in multiple sclerosis treated with alemtuzumab. *Mult. Scler.* 19(2), 241–244 (2013).

127 Fazekas F, Ropele S, Enzinger C, Seifert T, Strasser-Fuchs S. Quantitative magnetization transfer imaging of pre-lesional white-matter changes in multiple sclerosis. *Mult. Scler.* 8(6), 479–484 (2002).

128 Filippi M, Agosta F. Magnetization transfer MRI in multiple sclerosis. *J. Neuroimaging* 17(Suppl. 1), S22–S26 (2007).

129 Aharoni R, Vainshtein A, Stock A *et al.* Distinct pathological patterns in relapsing–remitting and chronic models of experimental autoimmune enchephalomyelitis and the neuroprotective effect of glatiramer acetate. *J. Autoimmun.* 37(3), 228–241 (2011).

130 Aharoni R, Eilam R, Domev H, Labunskay G, Sela M, Arnon R. The immunomodulator glatiramer acetate augments the expression of neurotrophic factors in brains of experimental autoimmune encephalomyelitis mice. *Proc. Natl Acad. Sci. USA* 102(52), 19045–19050 (2005).

131 Haacke EM, Xu Y, Cheng Y-CN, Reichenbach JR. Susceptibility weighted imaging (SWI). *Magn. Reson. Med.* 52(3), 612–618 (2004).

132 Chavhan GB, Babyn PS, Thomas B, Shroff MM, Haacke EM. Principles, techniques, and applications of T2*-based MR imaging and its special applications. *Radiographics* 29(5), 1433–1449 (2009).

133 Haacke E, Mittal S, Wu Z, Neelavalli J, Cheng Y-C. Susceptibility-weighted imaging: technical aspects and clinical applications, part 1. *Am. J. Neuroradiol.* 30(1), 19–30 (2009).

134 Gaitán MI, De Alwis MP, Sati P, Nair G, Reich DS. Multiple sclerosis shrinks intralesional, and enlarges extralesional, brain parenchymal veins. *Neurology* 80(2), 145–151 (2013).

135 Qian P, Cadavid D, Wolansky LJ, Cook SD, Naismith RT. Heterogeneity in longitudinal evolution of ring-enhancing multiple sclerosis lesions. *Ann. Neurol.* 70(4), 668–669 (2011).

136 Gaitán MI, Shea CD, Evangelou IE *et al.* Evolution of the blood–brain barrier in newly forming multiple sclerosis lesions. *Ann. Neurol.* 70(1), 22–29 (2011).

137 Haacke EM, Makki M, Ge Y *et al.* Characterizing iron deposition in multiple sclerosis lesions using susceptibility weighted imaging. *J. Magn. Reson. Imaging* 29(3), 537–544 (2009).

138 Van AT, Holdsworth SJ, Bammer R. *In vivo* investigation of restricted diffusion in the human brain with optimized oscillating diffusion gradient encoding. *Magn. Reson. Med.* 71(1), 83–94 (2014).

139 Cheung MM, Hui ES, Chan KC, Helpern JA, Qi L, Wu EX. Does diffusion kurtosis imaging lead to better neural tissue characterization? A rodent brain maturation study. *NeuroImage* 45(2), 386–392 (2009).

140 Zhang H, Schneider T, Wheeler-Kingshott CA, Alexander DC. NODDI: practical *in vivo* neurite orientation dispersion and density imaging of the human brain. *NeuroImage* 61(4), 1000–1016 (2012).

141 Van Essen DC, Ugurbil K, Auerbach E *et al.* The Human Connectome Project: a data acquisition perspective. *NeuroImage* 62(4), 2222–2231 (2012).

142 Maramraju SH, Smith SD, Junnarkar SS *et al.* Small animal simultaneous PET/MRI: initial experiences in a 9.4 T microMRI. *Phys. Med. Biol.* 56(8), 2459 (2011).

143 Cho ZH, Son YD, Choi EJ *et al. In vivo* human brain molecular imaging with a brain-dedicated PET/MRI system. *MAGMA* 26(1), 71–79 (2013).